Glacial overdeepenings in the Swiss Alps and foreland: Spatial distribution and morphometrics

Fabio Magrani, Pierre Valla, Natacha Gribenski, Elena Serra

Quaternary Science Reviews 243 (2020) 106483

Contents lists available at ScienceDirect

Quaternary Science Reviews

journal homepage: www.elsevier.com/locate/quascirev

Glacial overdeepenings in the Swiss Alps and foreland: Spatial distribution and morphometrics

Fabio Magrani [a, *], Pierre G. Valla [b, a], Natacha Gribenski [a], Elena Serra [a]

[a] Institute of Geological Sciences and Oeschger Centre for Climate Change Research, University of Bern, Baltzerstrasse 1, CH-3012, Bern, Switzerland
[b] Institute of Earth Sciences (ISTerre), Université Grenoble Alps, Université Savoie Mont Blanc, CNRS, IRD, IFSTAR, 38000, Grenoble, France

ARTICLE INFO

Article history:
Received 9 April 2020
Received in revised form
7 July 2020
Accepted 10 July 2020
Available online xxx

Keywords:
Glacial overdeepenings
Swiss alps and foreland
Morphometrics
Patterns of glacial erosion
(Sub-)glacial processes

ABSTRACT

Overdeepenings (ODs) are erosional features that have been excavated below the regional sea/fluvial base level to produce closed topographic basins. Accessing bedrock topography and OD volume is often challenging. Hence, despite constituting major landscape features and being widespread in (paleo-) glaciated regions, ODs have been overlooked and the subglacial processes involved in their evolution have remained debated. In the Swiss Alpine foreland and valleys, ODs are commonly found filled with water or large volumes of sediment. Using a GIS-Matlab approach based on topographic datasets and bedrock contour-curves, we mapped the spatial distribution of ODs in Switzerland and adjacent areas in the ice-free Alpine areas. The majority of the mapped ODs occurs in very-low bedrock erosional resistance, where ODs are larger, wider and shallower than in medium to high bedrock erosional resistance domains, evidencing a strong lithological control on OD geometry. Longitudinal asymmetry and hypsometric integral suggest a dominance of quarrying during OD evolution and, for selected glacial catchments, headward erosion propagation or high sediment evacuation efficiency. OD surface data (surface and length) can be tentatively used for extracting OD subsurface metrics (depths, nested valleys and first-order volume estimates). Our data seem to indicate that ODs may initiate as multiple small nested valleys and progress to a single and connected depression. Transversal cross-sections also suggest a negative feedback between the erosion potential for deep carving and the presence of low-resistance bedrock, where subglacial meltwater infiltration could have played a key role in OD evolution. Although insightful relationships have been evidenced for ODs in the Swiss Alps and foreland, we have also observed a high spatial variability in key OD metrics such as surface area and depth. This results in general (first-order) interpretations at regional scale, but currently prevent to quantitatively constrain physical subglacial processes at their origin. Comparisons with existing OD datasets under present-day ice (Greenland, Antarctica and modern Swiss glaciers) place our results in a broader context and allow a step forward in our understanding of the complex patterns and mechanisms of (sub-)glacial erosion and resulting landforms.

1. Introduction

The ability of glaciers to rapidly erode bedrock and shape the Earth's surface (Penck, 1905; Davis, 1906; Prasicek et al., 2015), from large valleys in mountain ranges (Hallet et al., 1996) to fjords (e.g., Glasser and Ghiglione, 2009), is evident worldwide (Egholm et al., 2009). As a consequence, scientific research has long focused on (paleo-)glacial geomorphology and glacial processes by investigating surface glacial landforms and deposits. However, major landforms produced by glacial erosion are hidden in the subsurface (i.e. below modern sediments, glaciers and waters), such as overdeepenings, that despite their geomorphological importance are still poorly studied and understood.

Overdeepenings (ODs) are large-scale erosional features, characteristic of glacially-sculpted landscapes (Carrivick et al., 2016; Haeberli et al., 2016; Patton et al., 2016). They have been defined as closed topographic depressions with adverse slopes in the direction of ice flow (Haeberli et al., 2016) and an 'overdeepened' bed below sea level or regional fluvial base level (Cook and Swift, 2012). These characteristics allow to distinguish ODs from 'glacially-deepened' valleys, which have not been excavated enough below the regional

* Corresponding author.
E-mail address: fabio.magrani@geo.unibe.ch (F. Magrani).

https://doi.org/10.1016/j.quascirev.2020.106483

base-level to create a closed topographic basin, while ODs require both ice and water at the glacier bed to traverse a locally-reversed (or adverse) subglacial slope (e.g., Cook and Swift, 2012).

ODs have the potential to store large volumes of water and sediment (e.g., Jansson et al., 2003; Preusser et al., 2010), being relevant for hydropower production, natural hazards assessment, geotechnical management and as potential sites for future lake formation (e.g., Fischer and Haeberli, 2012; Linsbauer et al., 2012; Magnin et al., 2020). From a glacio-geomorphological perspective, the presence of ODs is directly related to ice dynamics, erosion potential and sediment transport. ODs formation and long-term evolution require further consideration to better constrain ice-erosion models (e.g., Egholm et al., 2012) and improve our understanding of glacier and marine ice-sheet instabilities (e.g., Jones et al., 2015; Patton et al., 2016) and glacial/post-glacial landscape evolution (Cook and Swift, 2012). Therefore, identifying OD morphometric properties appears crucial for improving our understanding of ice dynamics and its impact on the Earth's topography.

OD origin and development have been suggested to result from a combination of direct glacial abrasion, quarrying (both deepening and widening; e.g., Hooke, 1991; Iverson, 2012) and to some extent subglacial meltwater erosion (e.g., Herman et al., 2011; Creyts et al., 2013; Beaud et al., 2016; Ugelvig et al., 2016) operating over several glacial-interglacial cycles (e.g., Dürst Stucki et al., 2010; Preusser et al., 2010; Reber and Schlunegger, 2016). However, the relative contribution of these different mechanisms has been poorly constrained, and the direct role of subglacial meltwater has remained debated with little evidence for significant contribution to bedrock erosion (e.g., Beaud et al., 2016; Alley et al., 2019). Topographic irregularities at the glacier base, enhancing ice-surface crevassing and quarrying potential (Hooke, 1991), lithological spatial variations (Glasser et al., 1998) and/or pre-existing topographic conditioning including tectonics (e.g., Kessler et al., 2008; Glasser and Ghiglione, 2009) have also been invoked for promoting OD development.

It has been proposed that OD location along a valley profile preferentially coincides with the long-term equilibrium line altitude (ELA), where increased ice flux and basal sliding would enhance glacial erosion (Anderson et al., 2006). However, complex feedbacks between ice/water flow and erosion/sedimentation can produce localized and deep glacial erosion (Hooke, 1991; Alley et al., 2003) and, hence, may act as important controls on OD size and morphology (Cook and Swift, 2012; Patton et al., 2015). At larger-scale, the spatial occurrence of ODs is in general associated with laterally-constrained ice flow (i.e. tributary confluences and valley-constrictions; e.g., MacGregor et al., 2000; Cook and Swift, 2012; Patton et al., 2016), although OD features are also frequent in regions where (paleo-)ice flow was unconstrained, such as mountain forelands (e.g., Preusser et al., 2010), glacier termini (Egholm et al., 2012) and zones of lithological or bedrock-strength changes (Cook and Swift, 2012).

Despite several studies focusing on ODs, especially in formerly-glaciated regions, the processes involved in their evolution remain poorly understood (Fischer and Haeberli, 2012). Investigating OD morphometrics and spatial distributions, in connection with different geological and geomorphic controls, is therefore crucial to improve our understanding of OD development processes during successive glaciations (e.g., Preusser et al., 2010).

In this study, we focus on the characterization of glacial ODs in the European Alps, specifically in Switzerland and neighboring areas (France and Germany). While present-day glaciers in the Swiss Alps are only found at high elevations, the Swiss Alpine foreland and surrounding massifs were extensively glaciated during Quaternary glaciations. The thermal regime of Quaternary glaciers has remained debated (e.g., Seguinot et al., 2018), but they have left an impressive glacial imprint on the topography (e.g., Preusser et al., 2010; Dürst-Stucki and Schlunegger, 2013), shaping the landscape into the well-known present-day U-shaped valleys, horns and over-deepened basins filled by (post-)glacial sediment and/or water (i.e. lakes; Herman et al., 2011; Sternai et al., 2013; Cohen et al., 2017). We assessed the morphometric characteristics, geometric relationships and spatial distributions of identified ODs. Our objective is to provide first-order quantitative constraints to discuss how bedrock resistance, local and regional settings and internal subglacial mechanisms may control the location and geometry of the Quaternary overdeepenings. To that aim, we have designed an automated GIS-routine to identify and extract OD features using filtering criterions (adapted from Patton et al., 2015) based on bedrock topographic models derived from geophysical investigations, borehole data and geometric reconstructions (Dürst-Stucki and Schlunegger, 2013; Mey et al., 2016). Additionally, we explored how OD surface metrics could serve as potential proxies to estimate, through empirical relationships, hidden or indirect subsurface morphometric variables (e.g., volume). Finally, we investigated OD cross-profiles and characteristic parameters (i.e. form-ratios and b-coefficients; Harbor, 1992; Augustinus, 1995; Prasicek et al., 2015) with the overall aim to explore the 3D geometry of ODs and further discuss the potential driving mechanisms (glacial *vs*. fluvial) at their origin.

2. Material and methods

2.1. Datasets

Our morphometric approach uses multiple topographic and geomorphic datasets. These are based on two main datasets: the current surface topography and an original bedrock-elevation model (Fig. 1A and B, respectively). In addition, we also use supplementary datasets: LGM (Last Glacial Maximum ~20 ka; Ivy-Ochs et al., 2006) ice extent and elevation, Quaternary sediment infill and bedrock erosional resistance (Fig. 1A, C and 1D, respectively).

The current surface topography (Fig. 1A) uses the DHM25 Digital Elevation Model (provided by Swisstopo - Bundesamt für Landestopografie Swisstopo), derived from the National Map 1:25000, with 25-m spatial (horizontal) resolution and an average vertical error of 1.5–2 m for the foreland and low-relief areas, and 3–8 m for the Alpine massifs (from comparison with photogrammetric measurements). We hence combined the current surface topography with the hydrology dataset (Swiss Map Vector 500, Swisstopo) that is based on the National Map 1:500000.

In order to cover the entire study area, our bedrock-elevation model (Fig. 1B) combines three different sources that were integrated and result in a 100-m horizontal resolution raster. The sources include the bedrock-elevation models of Mey et al. (2016) (hereafter Model 1), Dürst-Stucki and Schlunegger (2013) (hereafter Model 2), and the 2019 release bedrock-elevation model by Swisstopo (extension of Model 2). Model 1 is a 90-m raster resolution obtained from a computational approach, assuming a geometric continuity between the current topographic surface (exposed) and the buried bedrock topography (Mey et al., 2016). Model 2 has been constructed from borehole data (complemented by geophysical methods) to derive bedrock contour lines at 10-m intervals subsequently interpolated to generate a 25-m resolution dataset (Dürst-Stucki and Schlunegger, 2013; Swisstopo).

We have evaluated the bedrock-elevation Models 1 and 2 against borehole data in central Switzerland (Geosound data from Geoportal des Kantons Bern; Fig. 2A). For other parts of Switzerland, no comparison was performed due to data-access limitations. One major topographic feature in Switzerland is the

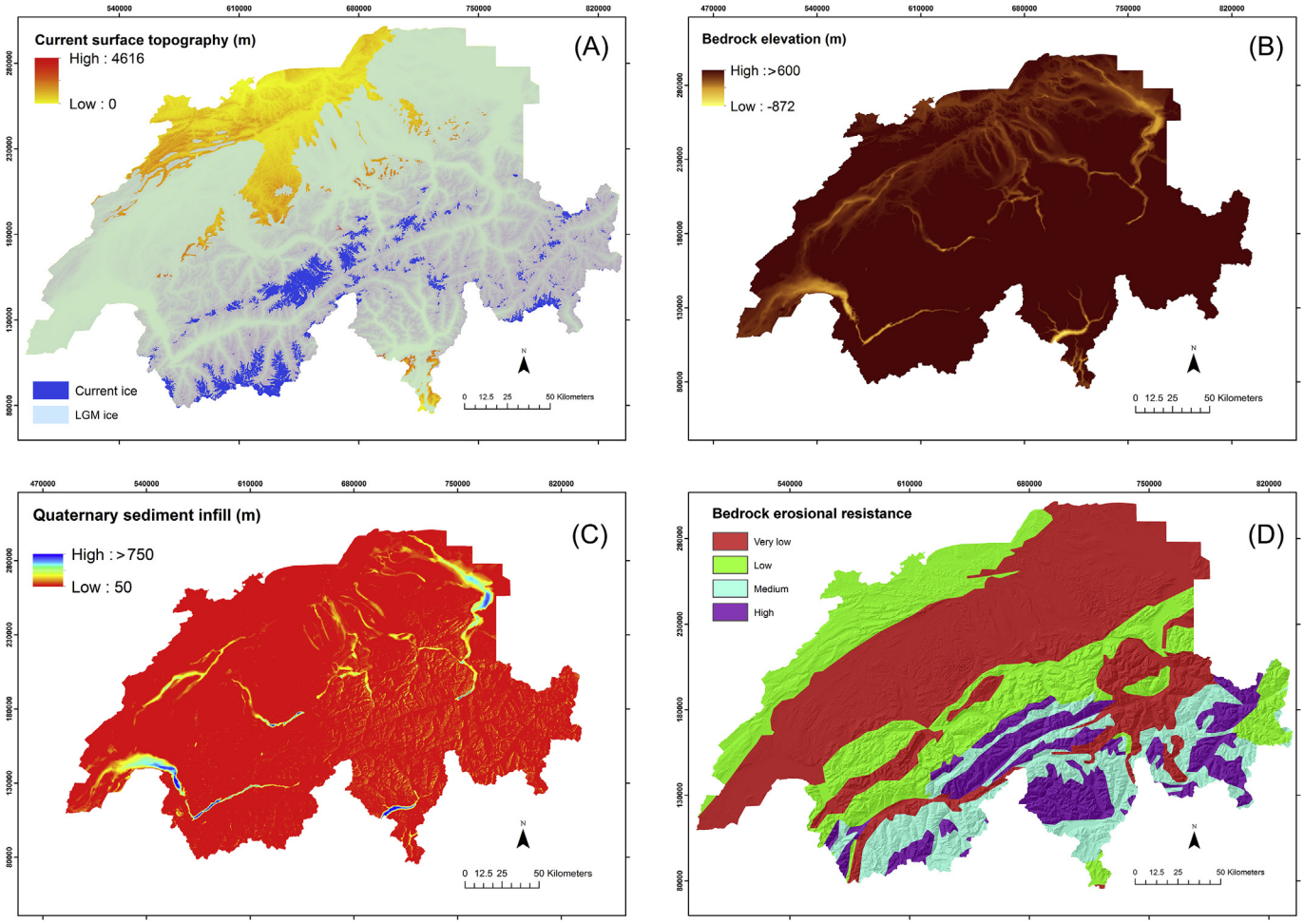

Fig. 1. Main GIS datasets for glacial overdeepenings in Switzerland. (A) Surface topography (DHM25, 25-m resolution, Swisstopo) with the current glacier coverage (GLIMS, 2005) and Last Glacial Maximum (LGM) ice extent (Bini et al., 2009). (B) Combined bedrock-elevation model based on different published datasets (Dürst-Stucki and Schlunegger, 2013; Mey et al., 2016) and on the 2019 Bedrock Elevation Model (Swisstopo). See text for details. (C) Calculated Quaternary sediment infill (including water for modern lakes) calculated from surface topography (A) and combined bedrock-elevation model (B). (D) Bedrock erosional resistance (Dürst-Stucki and Schlunegger, 2013) from the erodibility map (Kühni and Pfiffner, 2001). All coordinates are in UTM-32N, based on LV03, centered in Bern (600000, 200000). See text for bedrock elevation-model (B) and Quaternary sediment infill (C) calculations.

presence of an extensive foreland on the northern part (Fig. 1A), and the borehole cluster extends both in the foreland and mountainous regions. In this context, the bedrock-elevation models were split into "Foreland" (matching the Molasse Basin; after Sommaruga et al., 2012) and "Mountains" in order to evaluate each domain separately. With this approach, we aim to adopt the best combination of the two models (minimizing uncertainties in bedrock elevations) for our final bedrock-elevation model. In the Foreland, both models perform similarly, with more than 90% of the modelled bedrock-elevation data agreeing within ±50-m errors with borehole data (94% for Model 1 and 96% for Model 2; Fig. 2B). We note, however, that Model 1 tends to slightly underestimate true bedrock depth (mean error of −13.7 ±22.2m; Fig. 2B), compared to Model 2 (mean error of 2.4 ±22.1m). In the Mountains, both models slightly underestimate the true bedrock depth acquired from borehole data (mean error of −3.6 ±38.7m and −4.2 ±18.7m for Model 1 and 2, respectively), but Model 2 performs best, with 98% of the compared data within ±50-m errors, against 88% for Model 1 (Fig. 2C). We, thus, prioritized Model 2 to construct our bedrock-elevation model, where available, and filled the missing areas with data from Model 1 (Fig. 2A). Two additional key areas which were missing or incomplete in the Models 1 and 2 (Lake Luzern region and part of Upper Rhine; yellow outlines in Fig. 2A) were added using the 2019 release bedrock-elevation model by Swisstopo (which covers only some parts of Switzerland). We used a nearest-neighbor interpolator to build the final bedrock-elevation raster with 100-m horizontal resolution covering the entire Switzerland and the extended lake areas inside France and Germany (Fig. 1B). The Quaternary sediment infill map (Fig. 1C) was then produced through the subtraction of the bedrock elevation from the current surface topography dataset (DHM25; Fig. 1A), assuming a Quaternary origin for the bedrock topography and subsequent sediment filling (Fig. 1C).

A first-order estimate of LGM paleo-ice thickness (assuming full sediment infill during LGM conditions) across the study area was derived from the LGM ice-extent and elevation reconstruction of Bini et al. (2009). The LGM ice thickness was, therefore, based on the difference between the LGM ice elevation and the current topography (i.e. without adding the OD depths). This dataset (Swisstopo, Fig. 1A) is based on spatial interpolation of extensive mapping of paleo-glacial markers (e.g., erratics, glacial-polished bedrock and trimlines; e.g., Haeberli and Schlüchter, 1987; Florineth and Schlüchter, 1998; Ivy-Ochs et al., 2008; Braakhekke et al., 2016).

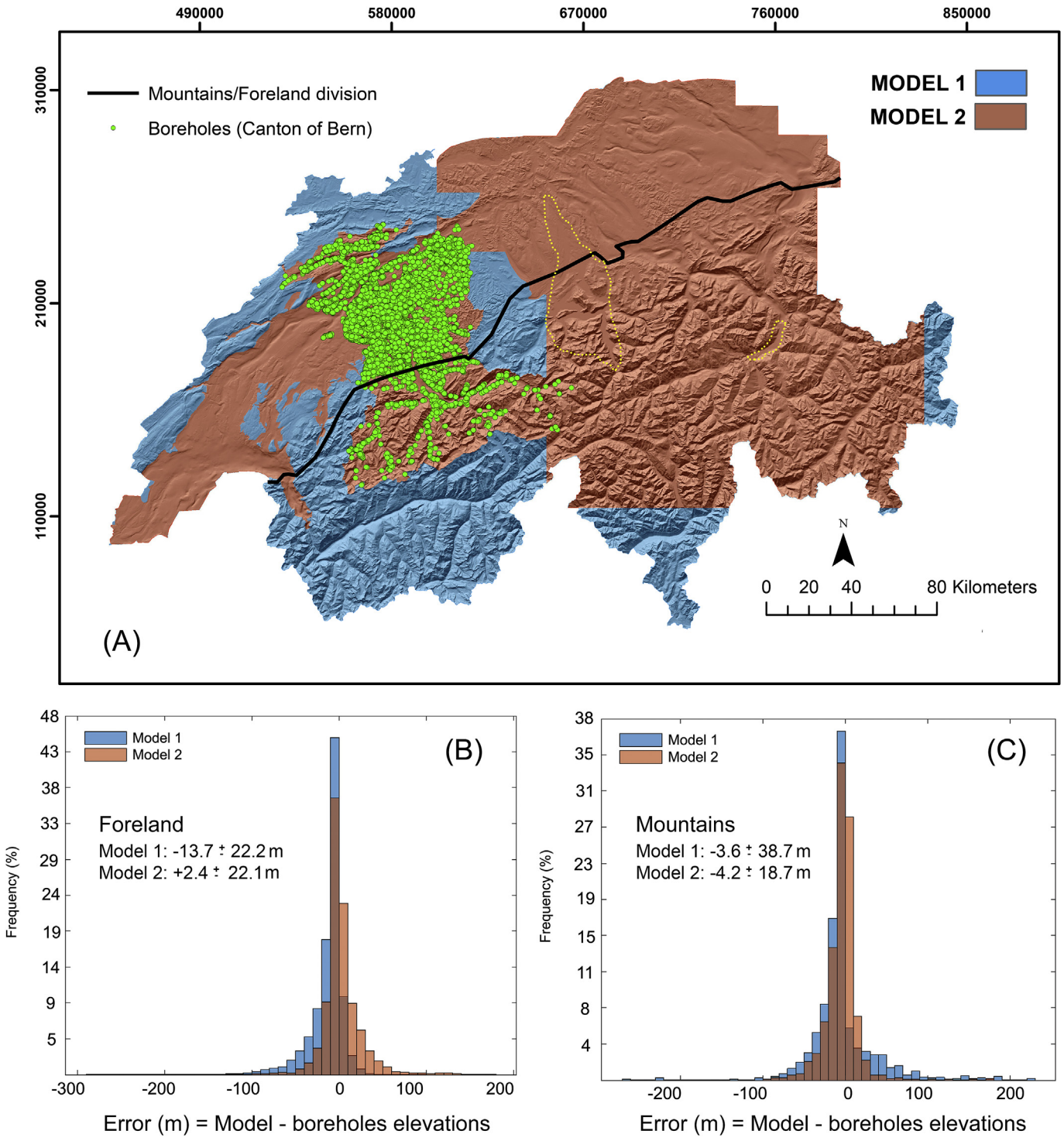

Fig. 2. Bedrock-elevation model validation. (A) Spatial distribution of bedrock-elevation models and available boreholes (green dots, Canton of Bern). Model 1 (blue) is adapted from Mey et al. (2016); Model 2 (red) is adapted from Dürst-Stucki and Schlunegger (2013). The black line geographically delimits the "Foreland" (which coincides with the Molasse Basin; after Sommaruga et al., 2012) and the "Mountains" domains. The yellow-dotted polygons represent the topographic areas where the new 2019 Bedrock Elevation Model by Swisstopo was used as an update for Model 2. Coordinates are in UTM, based on LV03, centered in Bern (600000, 200000). (B–C) Bedrock-elevation model deviations (Models 1 and 2) from borehole in the Foreland (B) and Mountains (C) areas. For each model and sector, the mean error values and standard deviations are derived from the error distributions. (For interpretation of the references to color in this figure legend, the reader is referred to the Web version of this article.)

Lastly, we used the bedrock erosional resistance map adapted from Kühni and Pfiffner (2001) (Fig. 1D), originally derived from the geotechnical map of Switzerland by Niggli and De Quervain (1936). The bedrock erosional resistance map is based on geological and geotechnical rock properties and boundaries following the main litho-tectonic contacts. Four classes have been re-categorized by Dürst-Stucki and Schlunegger (2013), from very-low to high bedrock erosional resistance (erodibility in Kühni and Pfiffner, 2001), and are used in the present study to investigate the first-order control of bedrock lithology on OD morphometric

parameters (Fig. 1D).

2.2. Methods: overdeepening delimitation (GIS-Matlab routine)

An automatic GIS-Matlab routine was designed in this study to spatially define ODs from our combined bedrock-elevation model. This GIS-routine builds on close procedures to the approach adopted by Patton et al. (2015), which consists in evaluating length changes in closed bedrock-contour curves while expanding from points of local elevation minima to identify closed depressions. This approach has the advantage to enable spatial analysis over large regions (i.e. the entire Switzerland and neighboring areas) while optimizing computer efficiency.

As a first step, a series of topographic masks based on different filtering criteria (sediment cover, topography, hydrology) are created to isolate points of local elevation minima from the bedrock-elevation model. The first mask (Mask 1; Fig. 3A) is delimited based on a sediment-thickness criterion: all cells whose Quaternary sediment infill is less than 20 m are removed from the bedrock-elevation model. The choice of the 20-m sediment-infill

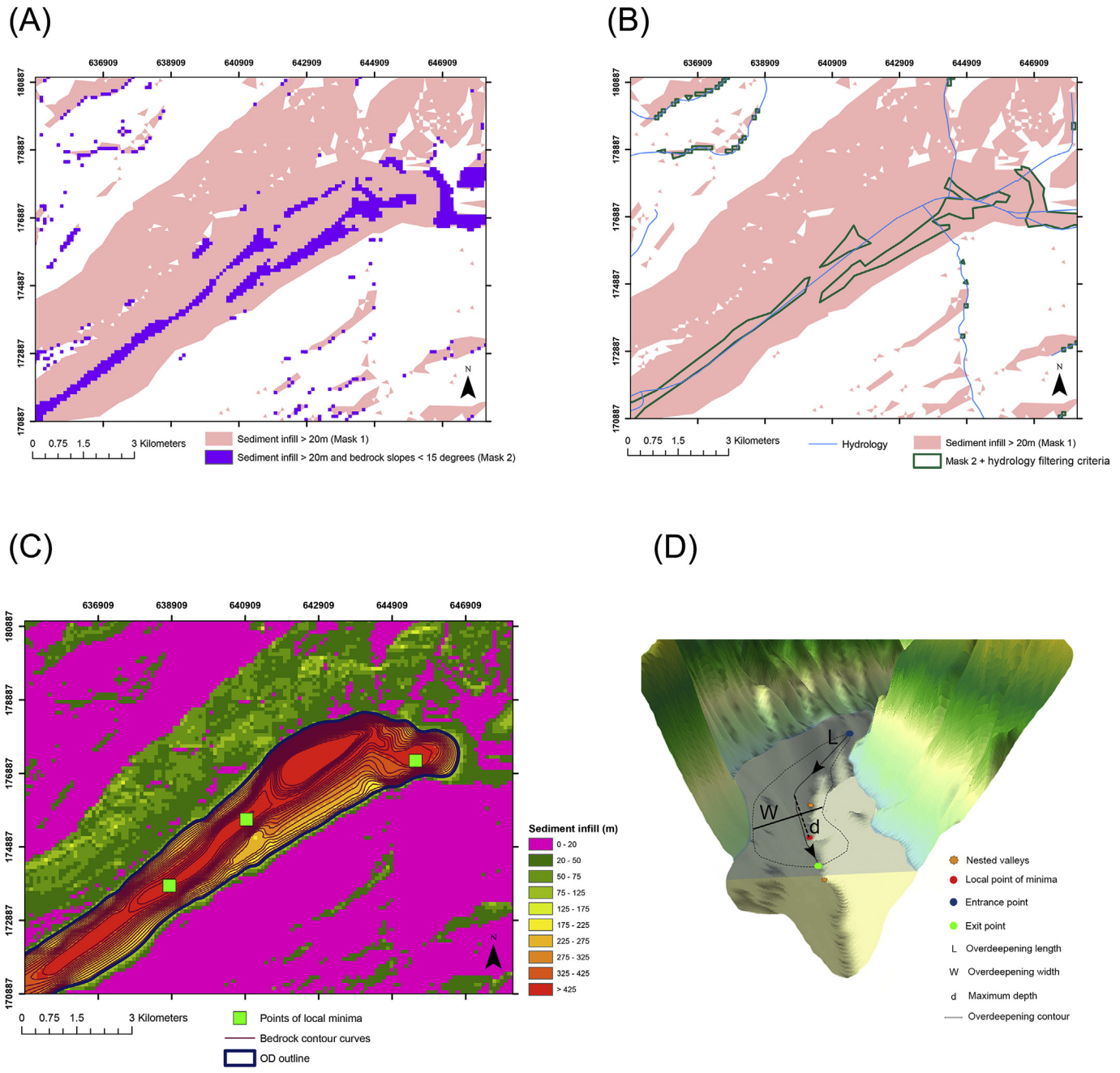

Fig. 3. Overdeepening (OD) characterization and selection trough bedrock-contour curves and multiple topographic masks (A-B-C). Example of combined bedrock model for methodology illustration. (A) First selection steps consider only bedrock-model cells whose sediment infill is higher than 20 m (Mask 1) and bedrock slopes lower than 15° (Mask 2). (B) Second filtering involves current hydrology (Swiss Map Vector 500, Swisstopo) to select drained areas. (C) Points of local minima are computed following the approach of Patton et al. (2015). The final shape of an OD is taken as the last bedrock contour (25-m elevation curves interval) inside Mask 1. (D) Example 3D view of the upper Aare valley (Canton of Bern) with the main location points (entrance and exit points, multiple local minima for identifying nested valleys) and main shape parameters (maximum depth, length and width). See text for discussion. All coordinates are in UTM, based on LV03, centered in Bern (600000, 200000).

threshold is conservative regarding our bedrock model's evaluation (Fig. 2B and C) and related to the original bedrock-elevation raster resolution (25 m; Dürst-Stucki and Schlunegger, 2013) with the further aim to remove both model artifacts from interpolation and very small sediment accumulations related to fluvial/hillslope processes. The second mask (Mask 2; Fig. 3A) applies a bedrock slope criterion: only cells with bedrock slopes below 15° are included (i.e. areas with low topographic gradients and thus encompassing preferably local elevation minima, Fig. 3A). The cell clusters remaining after filtering from Masks 1 and 2 are then converted into polygons (Fig. 3B, green outline) and a hydrology filtering is applied: polygons which are not crossed by the current hydrological network (Swiss Map Vector 500 from Swisstopo) are rejected. Assuming a first-order similarity between the present-day hydrological network and LGM ice-flow patterns, the application of this additional criterion allows to exclude areas where thick sediment accumulation (>20 m) is likely associated with other geomorphic processes (e.g., slope processes) than glacier dynamics. Points of local bedrock-elevation minima are then computed using zonal statistics for each individual polygon (Fig. 3C). Polygons whose points of local minima is associated to Quaternary sediment infill of less than 50 m are removed from our dataset, ensuring that the remaining polygons have at least one cell with 50 m of sediment infill (with 90% confidence based on our boreholes-model comparison, section 2.1).

In order to identify OD features, bedrock-elevation contour curves starting from each point of local minima are created using elevation increments of 25 m. Extremely large contour curves (perimeter longer than 600 km) were rejected to discard large tectonic/basin depressions, as well as very small depressions (perimeter smaller than 5 km). Using an original Matlab routine, final delimitations of ODs use the largest contour curves for each point of local minima (in a similar way as performed by Patton et al., 2015) contained within Mask 1 (sediment infill >20 m; Fig. 3C). In case of contours superposition due to multiple points of local minima (Fig. 3C), the longest contour is selected.

2.3. Morphometric parameters

For each OD in the study area, we have automatically extracted several morphometric parameters (Fig. 3D and Table S1). Main morphometric parameters include surface area (planar surface occupied by the OD), depth (mean and maximum depths, corresponding to the Quaternary sediment infill), width (longest cross-section, perpendicular to OD main direction), length (length of the OD flowline: line connecting the entrance and exit points through the maximum depth location) and elongation ratio (width divided by length). Geometric parameters based on cells counting were also considered, such as volume (for each individual cell area multiplied by the Quaternary sediment infill, based on a 100-m resolution raster) and bedrock hypsometric integral (bedrock depth distributions, as defined by Brocklehurst and Whipple, 2004).

We also extracted morphometric parameters characteristic of glacial ODs, such as the adverse slope (topographic gradient between the exit point and the closest point of local minima; Patton et al., 2016) and the longitudinal asymmetry (position of the deepest point along the OD flowline). An automated routine to detect and count the occurrence of nested valleys (small depressions along the flowline) was developed using a smoothing (Savitzky-Golay filter) of bedrock elevations along an OD flowline. Within this routine, we impose a minimum height-difference criterion of 50 m between the deepest point of the depression and the preceding peak (at least 1000 m distant from each other) to define a nested valley.

For large ODs (width greater than 400 m), we developed an automatic Matlab routine to extract bedrock and surface topography cross-sections (perpendicular to the OD flowline, using 500-m interval along the OD flowline and a sampling of 100-m interval along the cross-sections in order to smooth very small topographic changes). For each cross-section (1900 cross-profiles in total), we performed polynomial fitting to quantify the (U-)shape factor (b coefficient between 1 and 3, reflecting cross-section concavity; Harbor, 1992; Prasicek et al., 2015). In addition, we calculated the form ratio (ratio between cross-section depth and width; Harbor, 1992) and the transversal asymmetry (position of the local deepest point along the cross-section). Both the U-shape factor and form ratio have been used in order to quantify how much glacial erosion has modified the Swiss Alpine landscape (e.g., Harbor, 1992; Prasicek et al., 2015).

Finally, morphometric parameters (area, volume, depths, elongation, width and length) from modelled ODs under current ice (hereafter called Modern ODs) were also added to our dataset (hereafter called Quaternary ODs, including both the Foreland and the Mountains domains for ODs in currently ice-free areas). Modern OD morphometric data were based on Haeberli et al. (2016) and are derived from calculating ice thickness and bed topography below the present-day Alpine glaciers (Fig. 1A) using GlabTop (Linsbauer et al., 2009). In GlabTop, the ice thickness is calculated as a function of surface slope and interpolated with Inverse Distance Weight (IDK). For our study, we used the already processed morphometric parameters stored for the model run 2k_l2_Glabtop2 (Haeberli et al., 2016) to compare with morphometric data extracted from Quaternary ODs.

3. Morphometric results

3.1. Morphometric statistics and spatial distribution

For the entire study area, we have isolated 91 ODs in total, covering 6% of the total surface area (Fig. 4). The cumulated storage volume of the ODs corresponds to around 42% of the total Quaternary sediment infill volume of the region, calculated by subtracting the bedrock-elevation model from the present-day surface topography (Fig. 1C). A high concentration of Quaternary ODs (~80% of the total ODs area) can be observed in the Foreland. Such OD area distribution is mostly due to a few but very large individual ODs that accounts for most of the OD area and storage volume in the Foreland, in general associated to the main drainage systems (Fig. 4).

Fig. 5 illustrates the distributions of OD morphometric parameters. Filtering processes applied during the automatic OD delimitation have removed small topographic features (i.e. perimeter smaller than 5 km or maximum depth lower than 50 m), which is reflected in some asymmetric distributions or cut-off values in area (Fig. 5A), volume (Fig. 5C) and maximum depth (Fig. 5E). OD areas and volumes show similar histogram distributions, with a tendency to small areas (median = 3.2 km^2; Fig. 5A) and volumes (median = 0.44 km^3; Fig. 5C). The predominance of small ODs is also reflected in the tendency towards shallow depths, with around 73% of our ODs having maximum depths between 50 and 300 m (highly-skewed distribution for maximum depth with overall median = 180 m; Fig. 5E). Therefore, it is worth noting that our ±50-m error estimates (Fig. 2) can be significant, especially for shallow ODs (for our median OD depth of 180 m, this represents an uncertainty of ~28%). In general, Quaternary ODs tend to exhibit

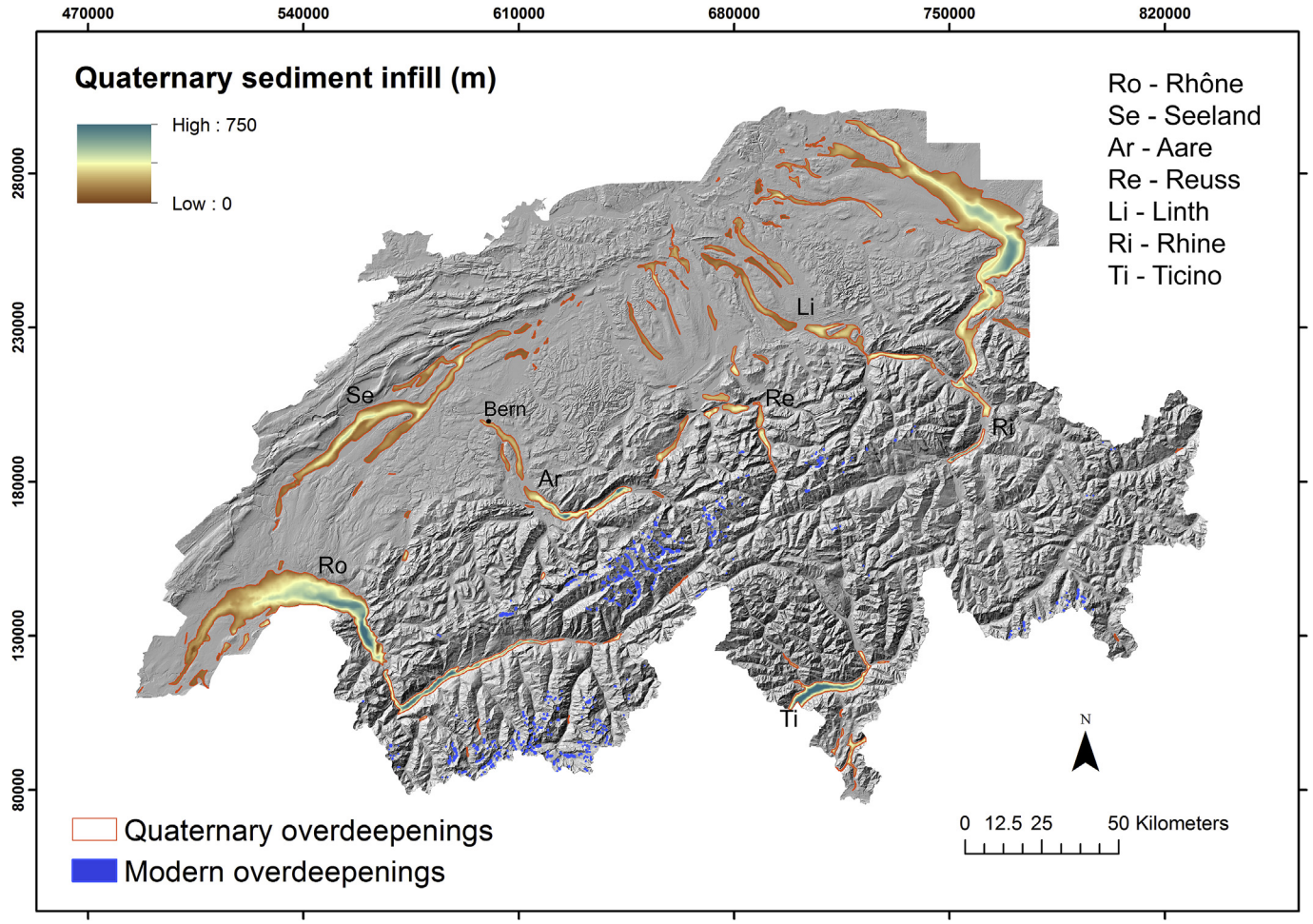

Fig. 4. Overdeepening outlines and sediment infills (including water for modern lakes) draped on hillshade DEM (DHM25, Swisstopo). Sediment infills are calculated trough the subtraction of the bedrock-elevation model with the present-day (surface) topography. Modern overdeepenings (i.e. currently under glaciers) are based on the dataset by Haeberli et al. (2016). The main drainages of Switzerland, Seeland region (after Dürst-Stucki and Schlunegger, 2013) and the city of Bern are indicated. Coordinates are in UTM, based on LV03, centered in Bern (600000, 200000).

low adverse slopes (highly-skewed distribution with overall median = 1.1°, Fig. 5B) and longitudinal asymmetries (no clearly-defined mode, but a dominance towards upstream asymmetries; Fig. 5F). Finally, hypsometric integral distribution shows a quasi-normal distribution (with one low-value outlier) centered around relatively high values (median = 0.58; Fig. 5D). Except for the maximum depths and adverse slopes, for which higher values are observed in the Mountains (Fig. 5B–E), other parameters show no significant differences between the Mountains and Foreland domains.

We also represented and categorized the main morphometric parameters in a georeferenced map to obtain potential information about their spatial variability (Fig. 6). In general, no specific spatial trend can be observed for the Quaternary ODs in terms of maximum depth, longitudinal asymmetry and number of nested valleys (Fig. 6C-E-F). On the other hand, largest OD volumes are mostly concentrated in the Foreland (Fig. 6A) and appear to be associated with lowest adverse slopes (Fig. 6B). The hypsometric integral is highly variable between ODs and locations. However, some patterns may emerge from contiguous ODs belonging to the same drainage catchments from the Mountains towards the Foreland, although these patterns differ between catchments (e.g., upper and lower Aare or upper and lower Rhône; Fig. 6D, locations in Fig. 4).

3.2. OD geometric relationships

We compared first-order morphometric parameters (e.g., area, depth, width, length) of ODs under current ice (modern ODs based on modelling; Haeberli et al., 2016) with ODs in ice-free areas (Quaternary ODs based on mapping; our dataset), with the overall aim to assess whether there might be geometric relationships and continuity between these two datasets. Both Modern and Quaternary OD datasets highlight a logarithmic relationship between area and maximum/mean depth (Fig. 7A and B), with a clear continuity between the two datasets for areas ranging over six orders of magnitude (Fig. 7). While 52% of the Quaternary ODs show maximum depths ranging from 50 to 200 m, all Modern ODs have maximum depths below 200 m (Fig. 7B). In addition, one striking observation is the very high variability in OD area and depth metrics, which has also been observed in other studies (e.g., Haeberli et al., 2016; Muñoz et al., 2020).

Similarly, a linear relationship ($r^2 \approx 0.8$) for both Modern and Quaternary ODs can be observed between OD length and width (Fig. 8A). The obtained linear trends between OD length and width suggest that ODs are in general significantly elongated (elongation

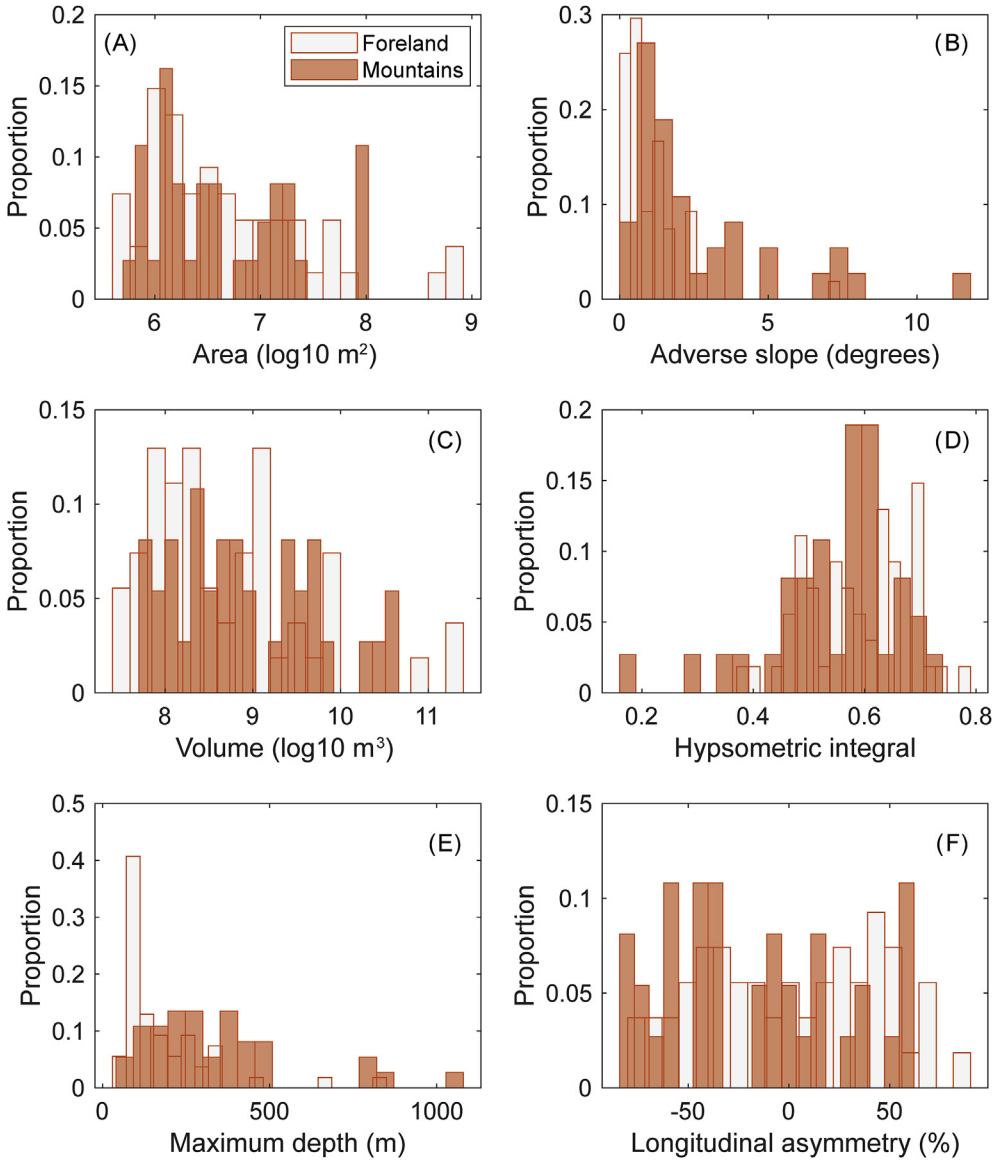

Fig. 5. Histograms of Quaternary overdeepening morphometrics (91 objects in total) for the Foreland and Mountains, with the different investigated parameters: (A) area; (B) adverse slope; (C) volume; (D) hypsometric integral; (E) maximum depth and (F) longitudinal asymmetry. See text for parameters definition and discussion.

ratio ~0.1; Fig. 8A). Furthermore, our observations on OD elongation ratio and area indicate that large ODs (area $>10^7$ m^2) tend to have low elongation ratios (<0.3), while smaller ODs present highly variable elongation ratios (from ~0.1 to 0.7; Fig. 8B).

3.3. OD controlling factors and predictive morphometrics

Fig. 9 illustrates the relationship between OD morphometrics and potential OD controlling factors (i.e. bedrock erosional resistance, LGM ice thickness). The majority of Quaternary ODs occurs in very-low (68%) and low (19%) resistive bedrock (which mostly coincides with the Foreland region; Fig. 1D). Investigation on depth *vs.* area/width relationships shows that ODs in very-low bedrock erosional resistance domains tend to be larger (i.e. bigger surface area; Fig. 9A), wider (Fig. 9B) and shallower (Fig. 9A and B), than ODs in medium to high bedrock erosional resistance domains, similar to the findings made by Augustinus (1992) and Swift et al. (2008) for glacial valleys in other settings. OD maximum depth appears positively correlated to maximum LGM ice thickness, with no apparent lithological control (Fig. 9C).

We investigated the relationship between OD surface (area and length) and subsurface (volume and nested valleys) metrics (Fig. 10). Mountains and Foreland domains can be also distinguished based on their difference in ice-flow regime (constrained and unconstrained ice flow, respectively). We observe a linear behavior between OD area and volume (Fig. 10A). Since OD volume and surface areas are linked, we would expect such a self-correlation as also pointed out by Muñoz et al. (2020). Considering that OD volume metric integrates depth, it is interesting to note similar OD area-volume relationship between Mountains and Foreland, suggesting a limited effect of the ice-flow setting on the OD depth distribution (Fig. 10A).

In addition, we found a direct (and linear) relationship between OD length and the number of nested valleys along the flowline, providing an empirical scaling relationship for our dataset (Fig. 10B). Interestingly, ODs with similar length present more

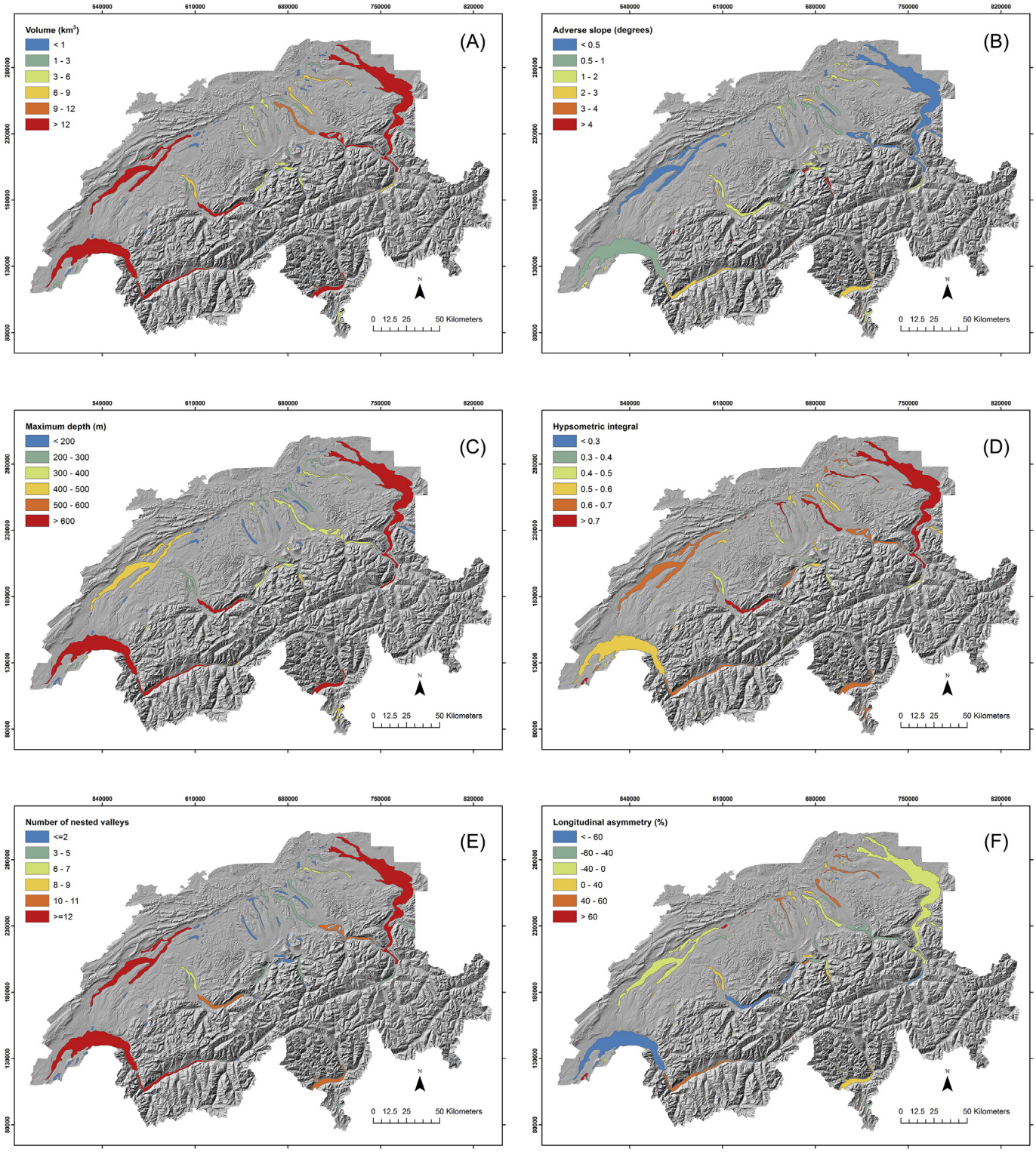

Fig. 6. Spatial patterns of Quaternary overdeepening morphometrics (91 objects in total) with the different investigated parameters: (A) volume; (B) adverse slope; (C) maximum depth; (D) hypsometric integral; (E) number of nested valleys and (F) longitudinal asymmetry. See text for parameters definition and discussion.

nested valleys in the Mountains (constrained ice flow) than in the Foreland (unconstrained ice flow). Nevertheless, these relationships, due to the intrinsic variability in OD metrics, are valid for regional-scale analysis in terms of orders of magnitude and may not be applicable for small-scale studies.

3.4. OD cross-sections

OD cross-section geometries have also been investigated for large ODs within our Quaternary OD dataset (OD width >400 m, excluding Modern ODs). 83 ODs have been selected in total and they occur both in the Foreland and Mountains domains (Fig. 11).

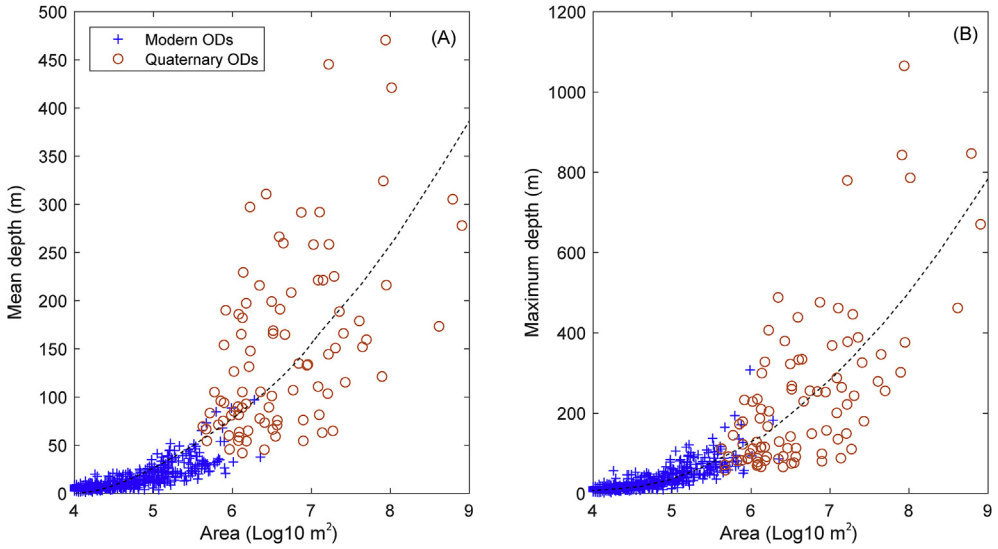

Fig. 7. Quaternary and Modern overdeepening area *vs.* mean (A) and maximum (B) depth. Similar logarithmic trends (best fits in dashed lines) are observed between the two datasets over six orders of magnitudes for OD areas.

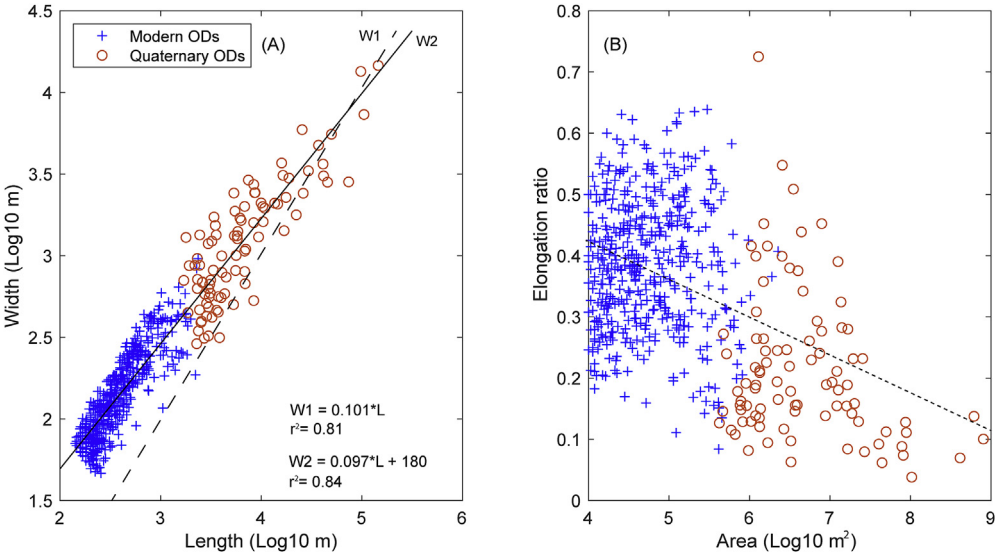

Fig. 8. Quaternary and Modern overdeepening length *vs.* width (A) and area *vs.* elongation ratio (B). A good continuity between Modern and Quaternary overdeepenings is observed over several orders of magnitudes for OD length (A) and area (B). Moreover, a linear relationship (A) is observed between OD length and width (r^2 = 0.81 and 0.84 with (W1) and without (W2) forcing through the origin, respectively). An exponential decreasing trend (B) is also observed between overdeepenings area and elongation ratio (best fit in dashed line). Note that data is presented in log-log scale for a better visualization, masking somehow the observed variability in OD metrics (although this generally does not exceed one order of magnitude).

We analyzed form-ratios and b coefficients in order to check the 3D evolution of the OD geometry along its longitudinal flowline (using, therefore, cross-sections), following the proposed metrics by Harbor (1992) and subsequent studies (e.g., Augustinus, 1995; Prasicek et al., 2015).

Histograms for OD cross-sections (averaged parameters over each individual OD) show a relatively symmetric distribution for the b coefficient (or shape-factor, median = 1.79; Fig. 11A), while the form ratio and elongation ratio distributions are largely skewed towards low values (medians = 0.09 and 0.18 respectively; Fig. 11B–D), reflecting the tendency of elongated and shallow overdeepenings. Low values of transversal-asymmetry were observed (median = 19.7%; Fig. 11C), suggesting in general symmetric OD cross-sections.

Averaged b coefficient variability for the 83 selected Quaternary ODs was investigated against area (Fig. 12A) and averaged form ratio (Fig. 12B), after distinguishing the ODs based on bedrock erosional resistance. At the scale of the entire OD dataset, no clear relationship can be observed between these cross-section parameters, nor any potential lithological control. However, we highlight that most of the ODs in very–low bedrock erosional resistance show an overall tendency to form ratios below 0.15 (Fig. 12B). When looking at the scale of individual ODs, there seem to be high spatial variability in the cross-section b coefficient and form ratio (Fig. 13). Fig. 13 shows two specific examples of OD cross-sections located in the upper Aare (low to very-low bedrock erosional resistance; Fig. 13A and B) and Ticino (high to medium bedrock erosional resistance; Fig. 13C and D), where opposite trends in b coefficient

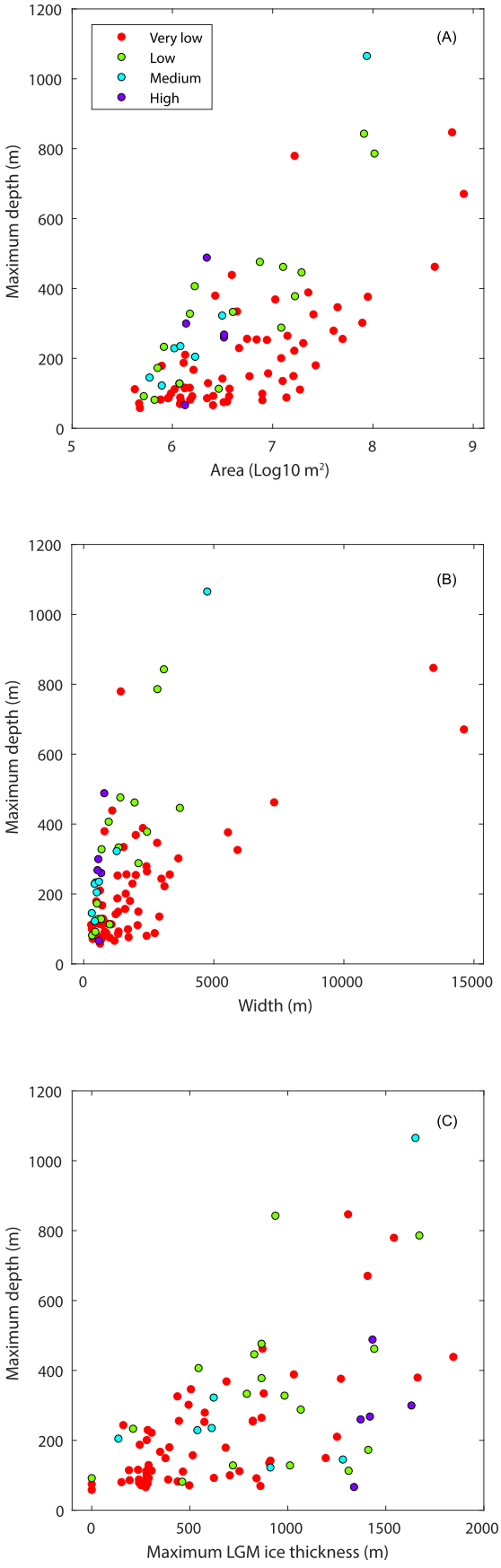

Fig. 9. Quaternary overdeepening maximum depth *vs.* area (A), width (B) and maximum LGM ice thickness (C). ODs are classified (color code) using the bedrock erosional resistance (Kühni and Pfiffner, 2001). While bedrock lithology seems to influence the geometrical relationships between area/width and maximum depth (A-B), bedrock resistance apparently does not modulate the observed apparent relationship between maximum LGM ice thickness and OD maximum depth (C). See text for discussion. (For interpretation of the references to color in this figure legend, the reader is referred to the Web version of this article.)

and form ratio are observed along their respective OD flowline. A slightly increasing to constant trend for the upper Aare (Fig. 13A) can be noticed for b coefficient, while Ticino shows a strong decreasing trend (Fig. 13C). From the form ratios, the upper Aare shows a decreasing trend along the OD flowline (Fig. 13B), while Ticino shows a slight increasing to constant downstream trend (Fig. 13D).

4. Discussion

4.1. Limitations and predictive morphometrics

In this section, we highlight some potential limitations of our selected datasets and approach for the delimitation of ODs and their consequences for the conducted morphometric analysis. We also provide some discussion on the potential usefulness of OD surface metrics (i.e. area and length) to extract information from the OD subsurface geometries (e.g., nested valley, volume).

4.1.1. Datasets and approach limitations

Our combined bedrock-elevation model (resolution of 100 m) smooths small bedrock topographic features due to downscaling (i.e. from 90-m resolution for Model 1 and 25-m resolution of Model 2). This computational step has direct effects on feature metrics derived from the combined bedrock-elevation model, such as the Quaternary sediment infill, OD delimitation and cross-sections (mostly b coefficients). Based on borehole evaluation (Fig. 2), we estimate that uncertainties up to ±50 m in bedrock elevations are probable. In other studied areas where borehole data was not available, our bedrock-model errors could not be estimated, but we hypothesize similar uncertainties. Besides, intrinsic assumptions of Model 1 for geometric continuity (Mey et al., 2016) include a positive relationship between valley width and subsurface infill thickness, leading to possible underestimates of true OD depth for narrow valleys. These limitations are also propagated in our analysis when using Model 1 (Fig. 2). Finally, it is worth noting that our derived Quaternary sediment infill (Fig. 1C) also overestimates true sediment thickness in lake-filled regions, while this does not affect our OD metrics.

Given that our OD delimitation approach used contour curves directly from the bedrock-elevation model with an imposed 25-m interval, the shape of each individual OD may slightly differ from reality (i.e. one contour curve difference). There are also possible limitations in our approach in respect to our filtering criteria. The hydrological dataset used for OD hydrology filter (Fig. 3B) is based on present-day river drainage and may inaccurately reflect the drainage pattern during the formation of ODs (i.e. during glacial conditions), and in addition this dataset does not include small rivers. Such uncertainties in the hydrology filtering may have led to dismiss small ODs from our dataset. However, the regional OD pattern and major ODs have not been affected by such criteria. Sensitivity tests were conducted for other topographic filtering, including minimum sediment infills (Mask 1) and bedrock slopes (Mask 2) (Fig. 3A). We have performed quantitative and qualitative tests for these parameters. Final threshold values of 20 m and 15°, respectively (Fig. 3A) have been adopted. Taking bedrock-elevation model errors into account, these threshold values have resulted in the removal of small OD features. We also highlight that possible

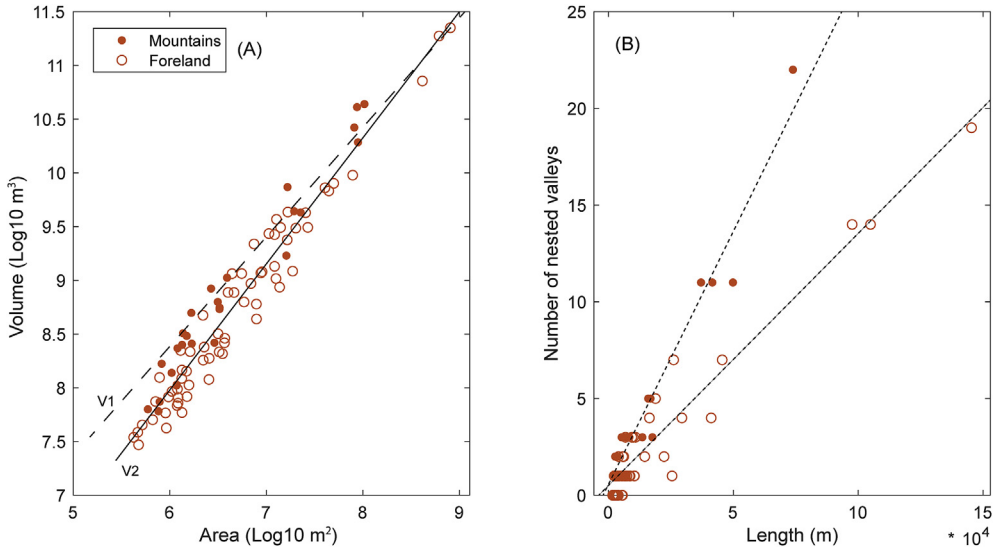

Fig. 10. (A) Quaternary overdeepening area *vs.* volume. The observed linear correlation between OD area and volume show no major difference between the Foreland and the Mountains, where ice flow is constrained. (B) Quaternary overdeepening length *vs.* number of nested valleys. The ice-flow type (*i.e.* constrained *vs.* unconstrained, respectively, in the Mountains and Foreland areas) appears to modulate the occurrence of nested valleys along an OD longitudinal profile. For the same length, ODs in the Mountains show a higher number of nested valleys when compared to the ones in the Foreland (dotted lines for illustration, best-fit linear trends).

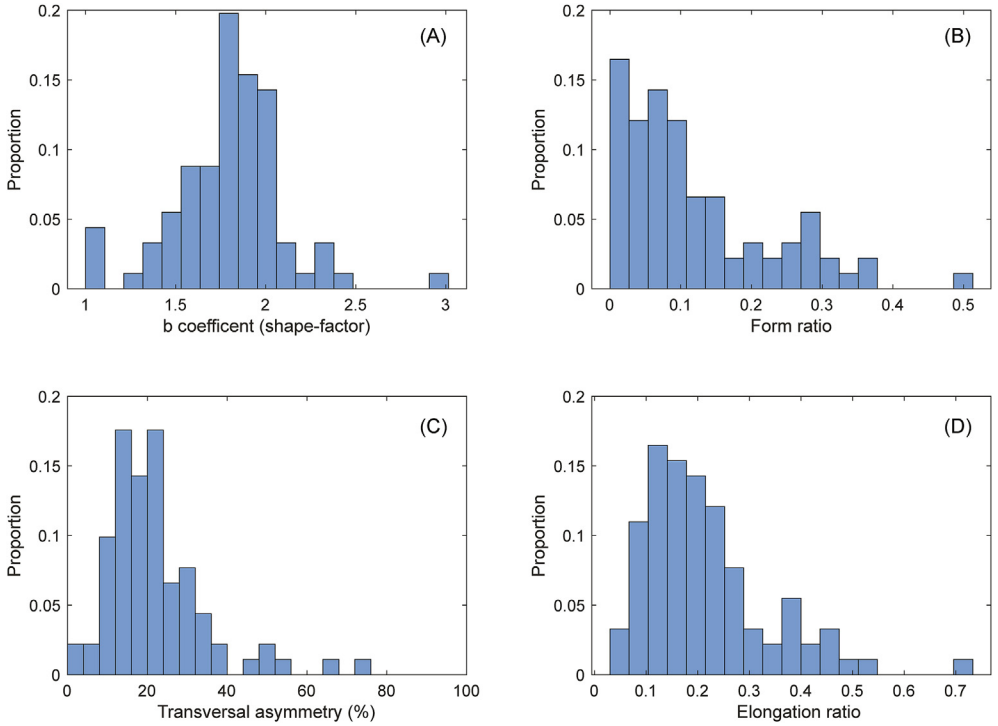

Fig. 11. Morphometric cross-section histograms of selected overdeepenings (83 objects in total, see text for selection criteria): (A) b coefficient (shape-factor); (B) form ratio; (C) transversal asymmetry and (D) elongation ratio. See text for parameters definition and discussion.

changes in the OD delimitation would occur when adopting different threshold parameters. These changes would have affected proportionally all the metrics (area, width, length) and therefore spatial patterns in OD geometry are not expected to vary significantly depending on the selected contour for final OD shape. As for the filtering criteria, we believe that these do not constitute a major limitation, since they are applied only to the points of local bedrock-elevation minima (Masks 1 and 2; Fig. 3A–C). Therefore, the most representative ODs in the Swiss Alps and foreland are kept with our conservative approach, whereas small OD features and potential topographic noise are removed from the bedrock-elevation models.

Assumptions were made also for the maximum LGM ice thickness calculation and the bedrock erosional resistance datasets (Fig. 1A and D), mainly for large-scale analysis purposes. The maximum LGM ice thickness was computed assuming full sediment infill during LGM conditions. We calculated LGM ice thickness for each OD cell by the difference between the LGM ice surface (Fig. 2A) and the current topography. With such a conservative

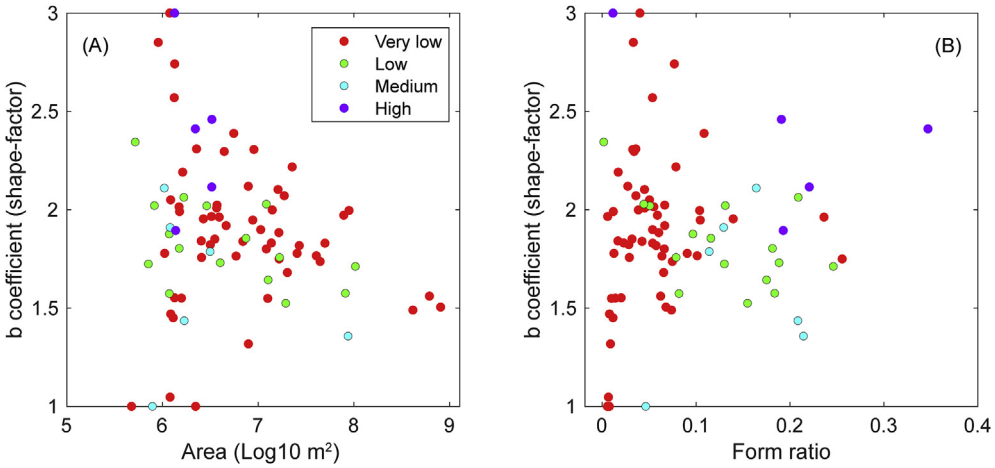

Fig. 12. Quaternary overdeepening cross-section morphometrics. (A) OD area *vs.* averaged cross-section b coefficient (shape-factor) colored by bedrock erosional resistance (see legend for color code; Kühni and Pfiffner, 2001). (B) Averaged cross-section form ratio *vs.* b coefficient (shape-factor) colored by bedrock erosional resistance. (For interpretation of the references to color in this figure legend, the reader is referred to the Web version of this article.)

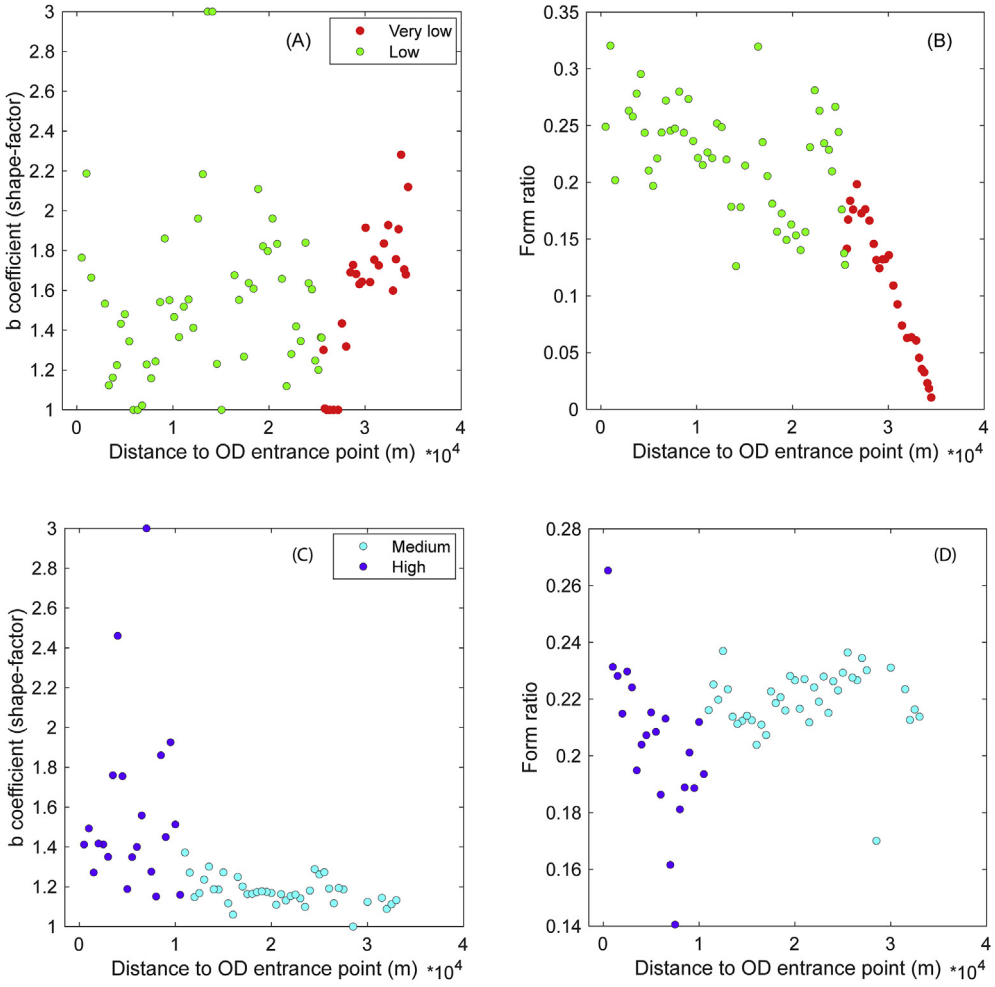

Fig. 13. Cross-section b coefficient (shape-factor) and form ratio along an OD profile line for two selected overdeepenings: upper Aare (A-B) and Ticino (C-D). See Fig. 4 for location. Each cross-profile is associated to the most representative bedrock erosional resistance (see legend for color code; Kühni and Pfiffner, 2001). Different distances between the points are due to quality control filtering that removed some cross-sections. (For interpretation of the references to color in this figure legend, the reader is referred to the Web version of this article.)

approach, we did not take into account OD depth into the calculation, preventing potential self-correlations in Fig. 9C. This may lead to an underestimate in true LGM ice thickness, especially for deep ODs that have been significantly excavated during LGM times

(Preusser et al., 2010). Concerning bedrock lithology, Kühni and Pfiffner (2001) summarized units with similar geotechnical resistance against mechanical and chemical weathering. This regional-scale bedrock erosional resistance map may, therefore, not reflect the local bedrock erosional resistance along OD cross-sections (Fig. 13). A higher-resolution bedrock erosional resistance map would optimize our cross-section results, although this would result in an increased lithological variability and associated difficulties for classification. In that sense, we believe that these results serve as a general first-order estimate for the lithological control on OD cross-sections.

At last, for OD cross-section computations, b coefficients are calculated as an average of the two OD sides for each cross-section. As a result, b coefficients tend towards low values for potential deep carving, even if slightly U-shaped. Besides, the averaging process may hide small differences among the two sides of an OD cross-section. This could mask the real shape at the OD bottom, but provides a homogenous approach for all cross-sections without the need for different topographic filterings.

4.1.2. Predictive morphometrics

Subsurface bedrock information is often difficult to access in (formerly-)glaciated areas, and OD metrics show often complex surface/subsurface relationships (e.g., Cook and Quincey, 2015). Thus, subsurface OD metrics are usually estimated for paleo-glacial environments or are empirically calculated for currently glaciated areas (e.g., Linsbauer et al., 2012). Haeberli et al. (2016) and Muñoz et al. (2020) highlighted the intrinsic complexity for establishing significant relationships between the different OD metrics due to their high variability. In this section, we investigate to what extent OD surface data (i.e. area and length, potentially easier metrics to obtain from topographic analysis) could serve as proxies for OD metrics subsurface (i.e. depth and volume calculated from them).

Although self-correlation can be expected between OD area and volume (Fig. 10A), we interestingly observe similar behaviors and scaling in both the Foreland and Mountains (Fig. 10A). This apparent similarity could be attributed to the fact that ODs in the Mountains are generally deeper (Fig. 5E), while Foreland ODs have preferentially larger surface areas (Fig. 5A). In this situation, it appears that the scaling observed between OD area and volume are not statistically different between the Mountains and Foreland.

The number of nested valleys, which could give an initial estimate on local erosion dynamics (i.e. child basins inside the parent overdeepening; Patton et al., 2015), show a relationship with OD length, but, in general, with a higher number of nested valleys for ODs located in the Mountains than in the Foreland (Fig. 10B). The higher number of tributary junctions in the Mountains, reflecting potential abrupt increase in ice discharge, could explain the observed difference. Moreover, although the locations of nested valleys do not exactly spatially occur at modern river confluences, we also observe a correlation between the number of nested valleys and the number of rivers confluences within an OD (using the current hydrology dataset, Table S1). This could indicate that nested basins and valley confluences are linked, which would support the nested valley origin depending on ice-flux and basal sliding increase (MacGregor et al., 2000; Cook and Swift, 2012; Haeberli et al., 2016). However, because topographically unconstrained settings coincide with the Molasse Basin (which comprises very-low bedrock erosional resistance), we cannot exclude that bedrock erosional resistance also plays a role in our observation. In this regard, in the Foreland ODs seem to develop fewer but bigger nested valleys than in the Mountains. Such evolution would evidence OD development from multiple small nested valleys to a single mature depression, following the conceptual model suggested by Patton et al. (2016).

4.2. Spatial relationships for Quaternary ODs

The spatial distribution of Quaternary ODs and their metrics in the Swiss Alps and foreland is widespread and relatively random (Fig. 4), but some trends can be observed. The Mountains show a clear trend for deeper ODs compared to the Foreland (Figs. 5E and 6C). The only exceptions in the Foreland are the Rhine and Rhône drainage systems. However, these extensive ODs have their deepest portions in their upstream parts, still within topographically constrained areas. Quaternary ODs with the biggest areas are mostly related to the major drainage systems (Fig. 4) and are concentrated in the Foreland (Fig. 5A), where they cross very-low resistive bedrock (Molasse Basin). On the other hand, in regard to volumes, the Seeland OD (Fig. 4) is the only OD entirely located in the Foreland with a volume above 12 km^3, where ice flow was possibly partially constrained by the Jura Mountains to the north during major glaciations (e.g., LGM; Bini et al., 2009). We observe similar spatial pattern for the number of nested valleys, that aside from the Seeland OD, are less present in the Foreland (Fig. 6E). Adverse slopes are slightly lower in the Foreland than in the Mountains (Fig. 5B) and associated to larger ODs (Fig. 6B). On the other hand, longitudinal asymmetry (Figs. 5F and 6F) shows no clear spatial relationship with the Foreland/Mountains domains or different drainage catchments, suggesting different controlling factor(s) for such geometric parameter.

Although we refer to these landscape features as Quaternary ODs with a glacial influence, we have no timing control for the OD formation and evolution, as already discussed in the literature (e.g., Preusser et al., 2010). In this sense, although hypsometric integrals are used mostly for discussing the maturity of surface landscapes (e.g., Brocklehurst and Whipple, 2004), we tested if such metric could provide information about the glacial imprint on subsurface topography and thus could help to estimate a first-order approximation for the timing of OD development. The Rhône and Aare ODs present higher hypsometric integrals in their upstream parts (Fig. 6D), showing a possible headward propagation of glacial erosion. Glacial modelling and erosion studies have also predicted such an upstream evolving erosion pattern (e.g., Shuster et al., 2011; Sternai et al., 2013). However, this proposed mechanism does not hold true for our whole dataset as we see reverse spatial patterns of hypsometric integrals for other major ODs (e.g., Linth and Rhine areas; Fig. 6D) Consequently, at the regional scale of our study, the high variability in hypsometric integral between and within ODs does not allow a possible estimate for the timing of OD development, remaining an open question for future investigation.

4.3. Comparison with other OD datasets

Morphometric parameters for Quaternary ODs in the Swiss Alps and foreland have similar distributions (Fig. 5) to ODs mapped by Patton et al. (2016) beneath Antarctica and Greenland ice sheets, potentially reflecting first our similar approaches for OD delimitation (Patton et al., 2015). Although absolute values may differ due to different glacial settings (ice sheets *vs.* alpine glaciers), surface (area, length and width) and subsurface (adverse slope and volume) metrics are largely skewed towards low values for all datasets (Fig. 5). Interestingly, maximum depths show similar absolute values and distributions for our dataset (Fig. 5E) and for Greenland/Antarctica (Patton et al., 2016). Median depths for Antarctica and Greenland ODs are 170–180 m, very similar to our dataset (180 m), and all datasets have ~25% of ODs shallower than 100-m deep. OD areas show much smaller medians for our dataset than ODs in

Antarctica or Greenland (medians of 3.2 km^2 *vs.* 137 km^2 and 74 km^2, respectively; Table S1; Patton et al., 2016). The dominance of small and shallow ODs in our Quaternary dataset (medians of 180 m and 3.2 km^2, respectively) could be attributed to insufficient growth time in the Swiss Alps (i.e. ice fluctuations during Quaternary glacial/interglacial periods) or the loss of erosional power (mostly in the Foreland, where ice flow diverges and glacier surface flattens). Our data show a slightly lower maximum depth range (up to 1000 m, compared to ~1500 m in Antarctica/Greenland datasets – Patton et al., 2016). From this perspective, even with the possible reduced availability of subglacial water in Antarctica and Greenland compared to the Swiss Alps, ODs have developed over long-term due to the stability of glacial conditions in polar settings. On the other hand, the confinement of ice within the narrow valleys from the Alpine region and increased water abundance could have led to an increased carving, compensating its reduced ice-cover duration. This would highlight that the erosional potential of ice sheets is enhanced mostly due to the longer permanence of ice and during warmer periods, as also suggested by Patton et al. (2016).

Longitudinal asymmetry shows a slight dominance towards negative values for 57% of our ODs (Fig. 5F), which may indicate a dominance of quarrying during OD evolution, since abrasion would act preferably at the exit point of ODs (Cook and Swift, 2012; Patton et al., 2016). In addition, subglacial fluvial processes could have also contributed to longitudinal asymmetry with spatially-variable efficiency in sediment evacuation and thus bedrock erosion (as also proposed in Patton et al., 2016), leading to a deeper upstream OD (high efficiency) and a sediment-covered adverse slope (low efficiency). The observed distribution is similar to that of Antarctica and Greenland, but our ODs show a slightly less skewed longitudinal asymmetry, with median of −7% *vs.* −21% and −22%, respectively for Antarctica and Greenland. Large drainage catchments that encompass several ODs (e.g., Aare or Rhône; Fig. 4), could evidence splitting of formerly contiguous ODs, resulting in preferentially negative values for longitudinal asymmetry (Fig. 6F).

Our dataset exhibits elongation ratios concentrated around 0.2 (Fig. 8B), which suggests that Alpine Quaternary ODs are more elongated than ODs in Antarctica and Greenland (median ~0.3; Patton et al., 2016) or Modern Alpine ODs (median ~0.4–0.5; Haeberli et al., 2016). This could be due to different local factors, such as structural pre-conditioning, or repeated glacial fluctuations (i.e. advance/retreat cycles) that may have affected more the Alpine Quaternary ODs, in comparison to the more stable ice sheets in Antarctica/Greenland or high-elevation Modern ODs.

Geometric relationships for area *vs.* maximum depths (Fig. 7B) in our study area showed a similar range (i.e. up to 1000 m for ODs <100 km^2) as Patton et al. (2016), but we observed a logarithmic instead of a linear trend. This behavior is closer to the one observed for Modern ODs in the Swiss Alps (Haerberli et al., 2016). The linear trend might be related to the km-scale size of ODs in Antarctica and Greenland, where ODs are not smaller than 10 km^2. Beyond this threshold, our OD dataset in the 10–100 km^2 range (Fig. 7B) could also be approximated by a linear fit as Patton et al. (2016) suggested for the Antarctica-Greenland dataset (10-10,000 km^2 range).

Alpine Quaternary OD length *vs.* width (Fig. 8A) showed a linear trend and overall relationship similar to the one found by Patton et al. (2016). Our observations indicate a 1:10 ratio between OD width and length, and appears to be slightly sensitive to local settings (i.e. Alpine *vs.* polar regions), since for Antarctica/Greenland the ratio is ~1:5. Although OD data present a high variability, we stress that this does not exceed one order of magnitude in general (Table S1). Such a generalized relationship could, thus, be used for future works that require simplification scaling (e.g., for ice modeling simulations).

Similar to the findings by Patton et al. (2016), no relationship was observed between adverse slope and maximum depth for the Alpine Quaternary ODs (Fig. 6B and C). Therefore, either downstream erosion (i.e. close to adverse slope) was mostly active during previous glaciations and minimal/none after the subsequent sediment infills, or the establishment of the adverse slope final gradient is not temporally synchronous to the deepest-point erosion inside an OD. The absence of connection between adverse slope and LGM ice thickness, might reinforce the idea that ODs were initially formed/developed during older glaciations than LGM when ice-thickness and extent were different. Our dataset shows that larger (and therefore longer) ODs present low-gradient adverse slopes, potentially linked to our methodological approach (taking the closest point of minima and the exit point for establishing the adverse slope) or reflecting sediment infills inside the OD that cannot be evacuated via the adverse slope, possibly shielding from further erosion (Alley et al., 1999). At last, the hypsometric integral (median = 0.58; Fig. 5D) could not be related to any of the main metrics available for our OD dataset, which implies that final OD geometries are a combination of local effects on the topography rather than a regional-scale erosional mechanism.

4.4. Controlling factors and dominant subglacial processes

In the present study, we have investigated the role of extrinsic factors in the development of glacial ODs, especially the influence of bedrock erosional resistance (Fig. 1D), ice-flow drainage (i.e. constrained *vs.* unconstrained flow in Mountains and Foreland, respectively, Fig. 2A) and maximum LGM ice thickness (Fig. 1A) as a proxy for late-Pleistocene ice flux and erosion potential (e.g., Anderson et al., 2006; Dürst-Stucki and Schlunegger, 2013).

Using the bedrock erosional resistance map allowed us to notice two different trends for OD width *vs.* maximum depth relationship, according to their bedrock erosional resistance class (Fig. 9B). ODs in very-low resistive bedrock tend to widen more than deepen, while in harder lithologies there is an inverse tendency with preferential deepening over valley widening. Such behavior has already been observed for ODs in ice-sheet settings (Patton et al., 2016) and fjords (Swift et al., 2008), and can be partially explained in our study by the fact that harder lithologies occur mostly in the Mountains (Fig. 1D). In the Mountains, tectonic deformation could have fractured the bedrock at depth (e.g., Dühnforth et al., 2010; Clarke and Burbank, 2011), providing bed irregularities that allow efficient erosion at the bottom of ice flow. Moreover, water-pressure in confined-flow situations may have enhanced quarrying and focus erosion at glacier beds (e.g., Rö;thlisberger & Iken, 1981; Jansson and Hooke, 1989). This situation may have been reinforced by subglacial fluvial processes, leading to high efficiency in sediment evacuation along the OD upstream part while sediment deposition occurred along the adverse slope (OD downstream part). Subglacial sediment transport, driven by subglacial water dynamics, is also an important controlling mechanism for large OD evolution which have a clear tendency towards low adverse slopes in both Alpine (Fig. 5) and polar (Cook and Swift, 2012) settings. Finally, topographically-constrained conditions (Mountains) have allowed greater ice accumulation, subglacial meltwater flux and, consequently, erosion. The relationship between OD depths and area (Fig. 7A and B) also supports this idea, with bigger ODs (i.e. associated with major drainage catchments) exhibiting increased depths, especially in harder lithologies. This highlights a possible important role of both the lithological and hydrological settings on OD deepening.

Another candidate for controlling OD morphometrics is the maximum LGM ice thickness. When analyzed against maximum depths (Fig. 9C), it shows an apparent exponential correlation,

although high variability is also observed. Several studies have highlighted the role of extensive ice masses in increasing erosion due to increased basal sliding (e.g., Cook and Swift, 2012; Egholm et al., 2012; Wang et al., 2018). The relationship we found here can allow a first-order estimate of OD maximum depth based on the reconstructed ice thickness. No lithological dependence in such relationship was evident for Quaternary ODs (Fig. 9C). Although LGM ice thickness can be used as a first-order proxy for OD maximum depth, it does not imply that the investigated ODs were formed during LGM time (Preusser et al., 2010). The absence of spatially-distributed ice thickness data from previous Quaternary glaciations, prevents a comparative analysis. Nevertheless, it is expected that during other Quaternary glaciations, the Alpine ice masses have been proportionally similar to the LGM (scaled up or down), maintaining the overall pattern and relationship we have evidenced.

4.5. OD transversal geometry and subglacial hydrology

Averaged cross-section b coefficients do not show any clear trend with area for the investigated ODs, and neither do they seem controlled by bedrock erosional resistance (Fig. 12A). On the other hand, cross-section form ratios show higher values for ODs located in harder lithologies and are associated to lower b coefficients (Fig. 12B). This may evidence that V-shaped cross-sections are in general deeper than their U-shaped equivalents, although this observed relationship is only qualitative and would require further investigation. Since we have presented here averaged values for all cross-sections within a given overdeepening, this could have masked the real trend. For this reason, in Fig. 13 we analyzed and reported each cross-section for two overdeepenings (see Fig. 4 for locations): upper Aare (Thunersee and Brienzsee) and Ticino (Lago Maggiore region). We have selected these key examples as they show opposite trends regarding b coefficients and form ratios along their flowlines.

For the upper Aare, b coefficients are variable along different cross-sections but they do not show any particular trend, ranging mostly from 1.2 to 2 (Fig. 13A). However, form ratios seem to show a bedrock shallowing trend downstream (i.e. decrease in form ratio; Fig. 13B), almost synchronously to a major lithological change (from Helvetic units/napes limestones to sub-alpine molasse/molasse sandstones; after Litty and Schlunegger, 2017). Simply put, a negative feedback is observed between the erosion potential for deep carving and the presence of low-resistance bedrock (i.e. Molasse Basin). This may be associated to subglacial water infiltration in the Molasse, reducing sliding and loosing erosional power (e.g., Beaud et al., 2014; Ugelvig et al., 2018; Steinemann et al., 2020). On the other hand, cross-sections from Ticino (Fig. 13C and D) show an opposite trend: b coefficients show a tendency towards V-shaped cross-sections downstream (i.e. low b coefficients; Fig. 13C), while form ratios are variable around 0.3–0.35. The transition from high to low b coefficients, is also occurring at a lithological contrast (i.e. from gneisses to granitoids/metasedimentary rocks). Such lithological contact also influenced the opposing trends of form ratios, with a decrease in variability when crossing from highly resistant to medium resistant bedrock (Fig. 13D). It should be emphasized that for the upper Aare, the OD entrance point is inside Lake Brienz and the exit point at the margins of Lake Thun, while the opposite occurs for Ticino: (entrance point at Lago Maggiore's margin and exit point inside the lake, here the OD is cut because of our model boundary). This could, alongside with opposite water pressure trends (decreasing for the upper Aare and increasing for Ticino), help explaining the observed opposing trends of form ratios (Fig. 13B *vs*. 13D). Moreover, due to the Messinian salinity crisis, the two catchments experienced very different glacio-fluvial histories (e.g., Bini et al., 1978; Finckh, 1978), which points towards a more glacially-influenced origin and development of the Aare OD, in contrast to a potentially more fluvial origin of the Ticino OD.

Since form ratios are based on the ratio between depths and widths (possibly masking changes in each individual metric), we also analyzed the relationship between depths *vs*. widths for each cross-section in the upper Aare and in the Ticino ODs (Fig. 14). In harder lithologies, depth *vs*. width seem to correlate well (Fig. 14C-D-F), suggesting that the Ticino overdeepening both deepens and widens. However, in the Aare OD, the width/depth pattern is less obvious, especially in the Molasse (Fig. 14E). Although width variability appears complex along the Aare OD (Fig. 14A), a shallowing is clearly noticeable (Fig. 14B). This would confirm a loss of erosional power at the OD bottom or a shift towards an increased lateral erosion in the Molasse low resistant bedrock, as also suggested in other glaciated settings (Augustinus, 1992, 1995; Swift et al., 2008).

Our interpretations for b coefficients or form ratios are based on cross-sections along OD profile (e.g., upper Aare *vs*. Ticino; Figs. 13–14), which could provide insights for their overall development. However, these specific observations cannot serve as quantitative estimates for glacial imprint on OD transversal geometry (Harbor, 1992), due to the variability encountered between analyzed cross-sections even within similar lithology. Moreover, other combined effects of subglacial processes, such as variations in water pressure and/or sediment shielding of bedrock, coupled with ice dynamics could have significant impacts on the depth and width evolution within ODs, and may explain the highly variable pattern observed in the Molasse Basin for the upper Aare OD (Fig. 14A-B-E). From our study, the use of cross-sections established at regular 500-m intervals along OD profile (i.e. not averaged) provides improved results when compared to averaged b coefficients and form ratios within each OD. On the other hand, the increased variability presents a challenge in accessing possible relationships between these morphometric parameters.

5. Conclusions

We have investigated, through a GIS Matlab-based approach for automatic OD delimitation, the morphometric characteristics, spatial patterns and relationships of Quaternary ODs in the Swiss Alpine foreland and neighboring areas. Together in comparison with ODs from other glaciated regions (Haeberli et al., 2016; Patton et al., 2016), our results provide some new perspectives on the possible controlling factors and the usage of surface proxies for subsurface OD metrics. Some key findings suggested by our data are summarized below:

1. The Quaternary ODs are major sediment storage features in the Swiss Alps and foreland (cumulated volume ~42% of the total sediment infill). The majority of Quaternary ODs occurs in very-low (68%) and low (19%) resistive bedrock, which mostly coincides with the Foreland region.
2. ODs in very-low bedrock erosional resistance domains tend to be larger, wider and shallower than in medium to high bedrock erosional resistance domains, which coincide with the Mountains region.
3. Maximum LGM ice thickness appears positively correlated to OD maximum depth, showing an exponential trend, but with no apparent lithological control on this relationship. This may reinforce the glacial origin for investigated ODs in Switzerland, although pre-glacial origin and more complex forming mechanisms cannot be excluded (Preusser et al., 2010), with the LGM ice pattern being a first-order proxy for older glacial periods during which the ODs were formed and evolved.

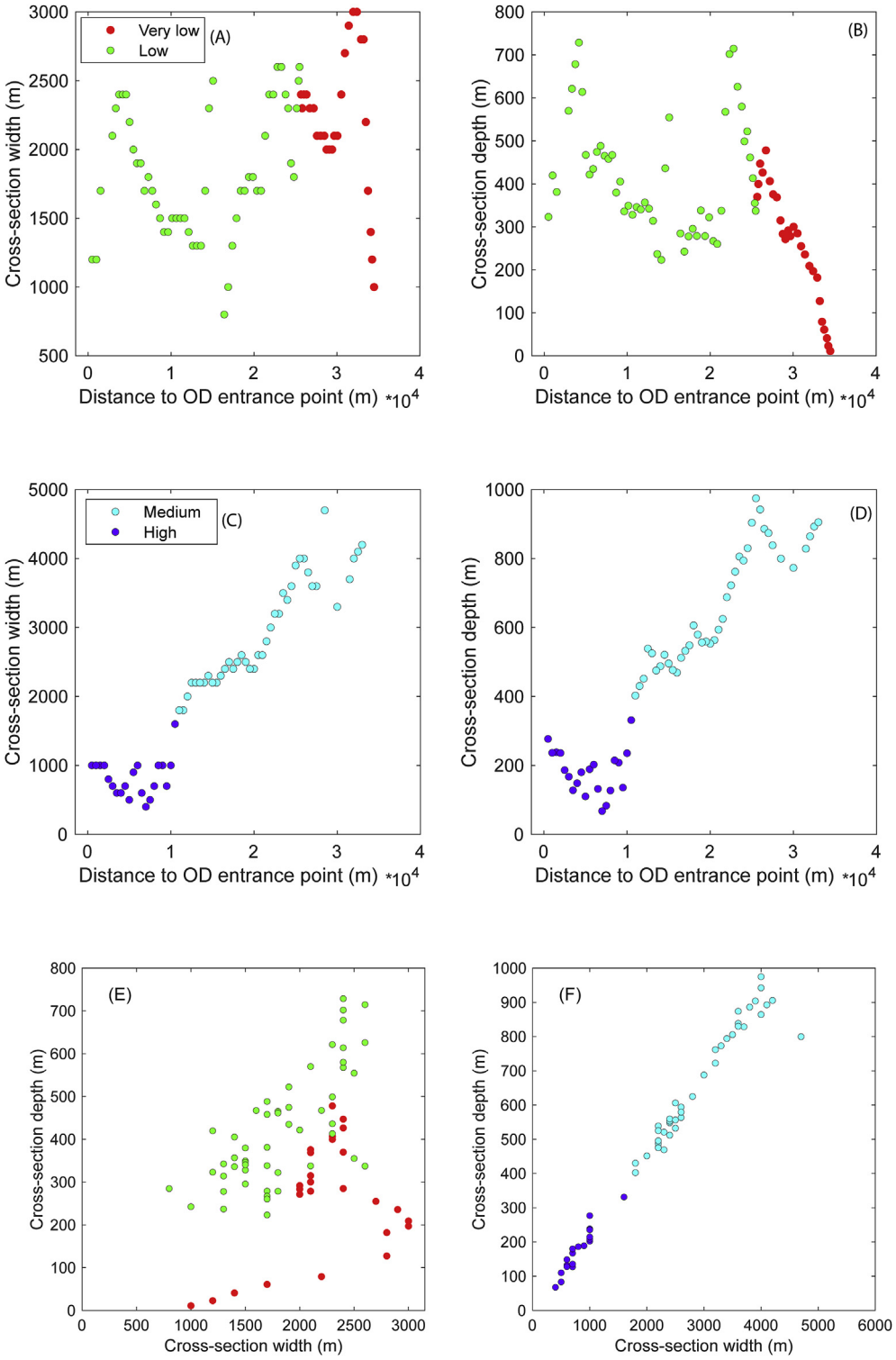

Fig. 14. Cross-section widths and depths for profiles along two selected overdeepenings: upper Aare (A-B) and Ticino (C-D). See Fig. 4 for location. Each cross-profile is associated to the most representative bedrock erosional resistance (see legend for color code; Kühni and Pfiffner, 2001) and the distance from the OD entrance point. Different distances between the points are due to quality control filtering that removed some cross-sections. The width/depth ratios are shown for the upper Aare (E) and Ticino (F), where remarkable differences can be noticed. (For interpretation of the references to color in this figure legend, the reader is referred to the Web version of this article.)

4. Maximum OD depths show similar absolute values and distributions for our dataset in comparison to Greenland and Antarctica (Patton et al., 2016). A comparison between area and maximum/mean depth show a logarithmic relationship for small ODs (our dataset, area <10 km^2) that can be approximated to a linear relationship for larger ODs (10-10,000 km^2). Due to the high variability in OD metrics, these relationships are suitable mainly for regional-scale studies where ODs are analyzed in terms of orders of magnitude and first-order processes.

5. Longitudinal asymmetry shows a slight dominance towards negative values (i.e. the OD deepest point is generally shifted upstream), which indicates a dominance of quarrying during OD evolution. Hypsometric integrals for selected catchments support headward erosion along major glacial catchments. Subglacial meltwater could also enhance the negative asymmetry by efficiently evacuating sediments towards the adverse slope.
6. Alpine Quaternary OD length *vs.* width show a linear trend, with a 1:10 width to length ratio. When compared with other regions, this ratio appears to be slightly sensitive to local settings (i.e. Alpine *vs.* polar regions). Indeed, our observations suggest that alpine Quaternary ODs tend to be more elongated than both Antarctica/Greenland ODs and Modern Alpine ODs, with characteristics resembling fjords (e.g., Swift et al., 2008).
7. A similar linear behavior between OD surface area and volume is observed, with high similarity for both constrained (Mountains) and unconstrained (Foreland) ice-flows.
8. Foreland ODs seem to develop fewer but bigger nested valleys than in Mountains. Such evolution would evidence ODs development from multiple small nested valleys to a single mature depression, following the conceptual model suggested by Patton et al. (2016).
9. Cross-sections along selected ODs show different spatial patterns that are apparently related to the lithological and hydrological settings. This is highlighted in the cross-section width *vs.* depth relationships. A negative feedback is observed between the erosion potential for deep carving and the presence of low-resistance bedrock (i.e. Molasse Basin) where infiltration of subglacial meltwater could have played a key role. This could have happened especially in the Foreland where meltwater abundance is reinforced by the basal thermal regime (i.e. warm-bed glacier) and ice flux convergence between glacial catchments.

Physical and numerical models based on 1D valley geometries and subglacial erosion processes can relatively simply explain the shape of ODs (e.g., Anderson et al., 2006; MacGregor et al., 2000). However, the real 3D shape and evolution of glacial ODs are more complex. Therefore, 3D numerical models (e.g., Egholm et al., 2012) computing ice dynamics and subglacial erosion, coupled with hydrology and sediment are essential. In this sense, our study provides quantitative data and morphometric relationships to allow the comparison between model outputs and morphometric observables. Such approaches can significantly improve our understanding of subglacial erosion and accordingly the physical laws within numerical models. In addition, the resolution and accuracy of bedrock topographic models is constantly improving thanks to geophysical data and borehole availability. We thus believe that future investigation will allow to move forward from our current interpretations, especially when combined with detailed lithological maps, enhancing the use of cross-section width and depths for 3D analysis of OD development. Finally, chrono-stratigraphic investigations, using geochronology techniques on sediment infills within ODs, would provide a major contribution to understanding the complex subglacial dynamics and erosion processes involved in ODs long term evolution.

Author contributions statement

Fabio Magrani and Pierre G. Valla: Conceptualization, methodology, formal analysis and writing. Natacha Gribenski and Elena Serra: Writing – review & editing, visualization.

Declaration of competing interest

The authors declare that they have no known competing financial interests or personal relationships that could have appeared to influence the work reported in this paper.

Acknowledgments

We thank A. Linsbauer for providing the dataset for the Modern Overdeepenings, and W. Haeberli and D. Swift for their constructive and insightful reviews. This study was supported by the Swiss National Science Foundation SNSF (Grant PP00P2_170559).

Appendix A. Supplementary data

Supplementary data to this article can be found online at https://doi.org/10.1016/j.quascirev.2020.106483.

References

Alley, R.B., Cuffey, K.M., Zoet, L.K., 2019. Glacial erosion: status and outlook. Ann. Glaciol. 1–3 https://doi.org/10.1017/aog.2019.38.
Alley, R.B., Lawson, D.E., Larson, G.J., Evenson, E.B., Baker, G.S., 2003. Stabilizing feedbacks in glacier-bed erosion. Nature 424, 758–760. https://doi.org/10.1038/nature01839.
Alley, R.B., Strasser, J.C., Lawson, D.E., Evenson, E.B., Larson, G.J., 1999. Glaciological and geological implications of basal-ice accretion in overdeepenings. In: Mickelson, D.M., Attig, J.W. (Eds.), Glacial Processes Past and Present, vol. 337. Geological Society of America Special Paper, pp. 1–9.
Anderson, R.S., Molnar, P., Kessler, M.A., 2006. Features of glacial valley profiles simply explained. J. Geophys. Res. Earth Surf. 111, 1–14. https://doi.org/10.1029/2005JF000344.
Augustinus, P.C., 1992. The influence of rock mass strength on glacial valley cross-profile morphometry: a case study from the Southern Alps, New Zealand. Earth Surf. Process. Landforms 17, 39–51.
Augustinus, P.C., 1995. Glacial valley cross-profile development: the influence of in situ rock stress and rock mass strength, with examples from the Southern Alps, New Zealand. Geomorphology 14, 87–97.
Beaud, F., Flowers, G.E., Pimentel, S., 2014. Seasonal-scale abrasion and quarrying patterns from a two-dimensional ice-flow model coupled to distributed and channelized subglacial drainage. Geomorphology 219, 176–191. https://doi.org/10.1016/j.geomorph.2014.04.036.
Beaud, F., Flowers, G.E., Venditti, J.G., 2016. Efficacy of bedrock erosion by subglacial water flow. Earth Surf. Dyn. 4, 125–145. https://doi.org/10.5194/esurf-4-125-2016.
Bini, A., Buoncristiani, J.-F., Couterrand, S., Ellwanger, D., Felber, M., Florineth, D., Graf, H.R., Keller, O., Kelly, M., Schlüchter, C., Schoeneich, P., 2009. Die Schweiz während des letzteiszeitlichen Maximums (LGM). Bundesamt für Landestopografie Swisstopo.
Bini, A., Cita, M.B., Gaetani, M., 1978. Southern Alpine lakes — hypothesis of an erosional origin related to the Messinian entrenchment. Mar. Geol. 27, 271–288. https://doi.org/10.1016/0025-3227(78)90035-X.
Braakhekke, J., Kober, F., Ivy-Ochs, S., 2016. A GIS-based compilation of the erratic boulders of the last glacial maximum in the Rhine glacier system. Natl. Coop. Dispos. Radioact. Waste Manag. Environ. Restor. 16–60.
Brocklehurst, S.H., Whipple, K.X., 2004. Hypsometry of glaciated landscapes. Earth Surf. Process. Landforms 29, 907–926. https://doi.org/10.1002/esp.1083.
Carrivick, J.L., Davies, B.J., James, W.H.M., Quincey, D.J., Glasser, N.F., 2016. Distributed ice thickness and glacier volume in southern South America. Global Planet. Change 146, 122–132. https://doi.org/10.1016/j.gloplacha.2016.09.010.
Clarke, B.A., Burbank, D.W., 2011. Quantifying bedrock-fracture patterns within the shallow subsurface: implications for rock mass strength, bedrock landslides, and erodibility. J. Geophys. Res. Earth Surf. 116 https://doi.org/10.1029/2011JF001987.
Cohen, D., Gillet-Chaulet, F., Haeberli, W., Machguth, H., Fischer, U.H., 2017. Numerical reconstructions of the flow and basal conditions of the Rhine glacier, European central alps, at the last glacial maximum. Cryosphere Discuss. 1–42 https://doi.org/10.5194/tc-2017-204.
Cook, S.J., Quincey, D.J., 2015. Estimating the volume of Alpine glacial lakes. Earth Surf. Dynam. 3, 559–575. https://doi.org/10.5194/esurf-3-559-2015.
Cook, S.J., Swift, D.A., 2012. Subglacial basins: their origin and importance in glacial systems and landscapes. Earth Sci. Rev. 115, 332–372. https://doi.org/10.1016/j.earscirev.2012.09.009.
Creyts, T.T., Clarke, G.K.C., Church, M., 2013. Evolution of subglacial overdeepenings in response to sediment redistribution and glaciohydraulic supercooling. J. Geophys. Res. Earth Surf. 118, 423–446. https://doi.org/10.1002/jgrf.20033.

Davis, W.M., 1906. The sculpture of mountains by glaciers. Scot. Geogr. Mag. 22 (2), 76–89.
Dühnforth, M., Anderson, R.S., Ward, D., Stock, G.M., 2010. Bedrock fracture control of glacial erosion processes and rates. Geology 38, 423–426. https://doi.org/10.1130/G30576.1.
Dürst Stucki, M., Reber, R., Schlunegger, F., 2010. Subglacial tunnel valleys in the Alpine foreland: an example from Bern, Switzerland. Swiss J. Geosci. 103, 363–374. https://doi.org/10.1007/s00015-010-0042-0.
Dürst Stucki, M., Schlunegger, F., 2013. Identification of erosional mechanisms during past glaciations based on a bedrock surface model of the central European Alps. Earth Planet Sci. Lett. 384, 57–70. https://doi.org/10.1016/j.epsl.2013.10.009.
Egholm, D.L., Pedersen, V.K., Knudsen, M.F., Larsen, N.K., 2012. Coupling the flow of ice, water, and sediment in a glacial landscape evolution model. Geomorphology 141–142, 47–66. https://doi.org/10.1016/j.geomorph.2011.12.019.
Egholm, D.L., Piotrowski, J.A., Lesemann, J., Nielsen, S.B., 2009. A finite-volume approach for coupled simulations of ice , sediment , and melt-water transport. Assembly 11, 4650.
Finckh, P.G., 1978. Are southern Alpine lakes former Messinian canyons? - geophysical evidence for preglacial erosion in the southern Alpine lakes. Mar. Geol. 27, 289–302. https://doi.org/10.1016/0025-3227(78)90036-1.
Fischer, U.H., Haeberli, W., 2012. Overdeepenings in Glacial Systems: Processes and Uncertainties, vol. 93. Eos, Washington. DC, p. 341. https://doi.org/10.1029/2012EO350010.
Florineth, D., Schlüchter, C., 1998. Reconstructing the last glacial maximum (LGM) ice surface geometry and flowlines in the central Swiss alps. Eclogae Geol. Helv. 91, 391–407.
Glasser, N.F., Crawford, K.R., Hambrey, M.J., Bennett, M.R., Huddart, D., 1998. Lithological and structural controls on the surface wear characteristics of glaciated metamorphic bedrock surfaces: Ossian sarsfjellet, svalbard1. J. Geol. 106, 319–329. https://doi.org/10.1086/516025.
Glasser, N.F., Ghiglione, M.C., 2009. Structural, tectonic and glaciological controls on the evolution of fjord landscapes. Geomorphology 105, 291–302. https://doi.org/10.1016/j.geomorph.2008.10.007.
GLIMS/NSIDC, 2005, updated 2019. Global land ice measurements from space glacier database. In: Compiled and Made Available by the International GLIMS Community and the National Snow and Ice Data Center, Boulder CO, U.S.A. https://doi.org/10.7265/N5V98602.
Haeberli, W., Linsbauer, A., Cochachin, A., Salazar, C., Fischer, U.H., 2016. On the morphological characteristics of overdeepenings in high-mountain glacier beds. Earth Surf. Process. Landforms 41, 1980–1990. https://doi.org/10.1002/esp.3966.
Haeberli, W., Schlüchter, C., 1987. Geological evidence to constrain modelling of the late pleistocene Rhonegletscher (Switzerland). Phys. Basis Ice Sheet Model 170, 333–346.
Hallet, B., Hunter, L., Bogen, J., 1996. Rates of erosion and sediment evacuation by glaciers: a review of field data and their implications. Global Planet. Change 12, 213–235.
Harbor, J.M., 1992. Numerical modeling of the development of U-shaped valleys by glacial erosion. Geol. Soc. Am. Bull. 104, 1364–1375. https://doi.org/10.1130/0016-7606(1992)104<1364:NMOTDO>2.3.CO;2.
Herman, F., Beaud, F., Champagnac, J.D., Lemieux, J.M., Sternai, P., 2011. Glacial hydrology and erosion patterns: a mechanism for carving glacial valleys. Earth Planet Sci. Lett. 310, 498–508. https://doi.org/10.1016/j.epsl.2011.08.022.
Hooke, R., 1991. Positive feedbacks associated with erosion of glacial cirques and overdeepenings. Geol. Soc. Am. Bull. 103, 1104–1108. https://doi.org/10.1130/0016-7606(1991)103<1104:PFAWEO>2.3.CO;2.
Iverson, N.R., 2012. A theory of glacial quarrying for landscape evolution models. Geology 40, 679–682. https://doi.org/10.1130/G33079.1.
Ivy-Ochs, S., Kerschner, H., Reuther, A., Maisch, M., Sailer, R., Schaefer, J., Kubik, P.W., Synal, H.A., Schlüchter, C., 2006. The timing of glacier advances in the northern European Alps based on surface exposure dating with cosmogenic 10 Be, 26 Al, 36 Cl, and 21 Ne. Spec. Pap. Geol. Soc. Am. 415, 43–60. https://doi.org/10.1130/2006.2415(04).
Ivy-Ochs, S., Kerschner, H., Reuther, A., Preusser, F., Heine, K., Maisch, M., Kubik, P.W., Schlüchter, C., 2008. Chronology of the Last Glacial Cycle in the European Alps, vol. 23, pp. 559–573. https://doi.org/10.1002/jqs.1202.
Jansson, P., Hock, R., Schneider, T., 2003. The concept of glacier storage: a review. J. Hydrol. 282, 116–129. https://doi.org/10.1016/S0022-1694(03)00258-0.
Jansson, P., Hooke, R.L., 1989. Short-term variations in strain and surface tilt on Storglaciaren, Kebnekaise, northern Sweden. J. Glaciol. 35, 201–208. https://doi.org/10.3189/s0022143000004512.
Jones, R.S., Mackintosh, A.N., Norton, K.P., Golledge, N.R., Fogwill, C.J., Kubik, P.W., Christl, M., Greenwood, S.L., 2015. Rapid Holocene thinning of an East Antarctic outlet glacier driven by marine ice sheet instability. Nat. Commun. 6, 8910.
Kessler, M.A., Anderson, R.S., Briner, J.P., 2008. Fjord insertion into continental margins driven by topographic steering of ice. Nat. Geosci. 1, 365–369. https://doi.org/10.1038/ngeo201.
Kühni, A., Pfiffner, O.A., 2001. The relief of the Swiss Alps and adjacent areas and its relation to lithology and structure: topographic analysis from a 250-m DEM. Geomorphology 41, 285–307. https://doi.org/10.1016/S0169-555X(01)00060-5.
Linsbauer, A., Paul, F., Haeberli, W., 2012. Modeling glacier thickness distribution and bed topography over entire mountain ranges with glabtop: application of a fast and robust approach. J. Geophys. Res. Earth Surf. 117, 1–17. https://doi.org/10.1029/2011JF002313.
Linsbauer, A., Paul, F., Hoelzle, M., Frey, H., Haeberli, W., 2009. The Swiss Alps without glaciers - a GIS-based modelling approach for reconstruction of glacier beds. Proc. Geomorphometry 243–247. https://doi.org/10.5167/uzh-27834, 2009.
Litty, C., Schlunegger, F., 2017. Controls on pebbles' size and shape in streams of the Swiss alps. J. Geol. 125, 101–112. https://doi.org/10.1086/689183.
MacGregor, K.R., Anderson, R.S., Anderson, S.P., Waddington, E.D., 2000. Numerical simulations of glacial-valley longitudinal profile evolution. Geology 28, 1031–1034. https://doi.org/10.1130/0091-7613(2000)028<1031:NSOGVL>2.3.CO;2.
Magnin, F., Haeberli, W., Linsbauer, A., Deline, P., Ravanel, L., 2020. Estimating glacier-bed overdeepenings as possible sites of future lakes in the de-glaciating Mont Blanc massif (Western European Alps). Geomorphology 350, 106913. https://doi.org/10.1016/j.geomorph.2019.106913.
Mey, J., Scherler, D., Wickert, A.D., Egholm, D.L., Tesauro, M., Schildgen, T.F., Strecker, M.R., 2016. Glacial isostatic uplift of the European Alps. Nat. Commun. 7, 1–10. https://doi.org/10.1038/ncomms13382.
Muñoz, R., Huggel, C., Frey, H., Cochachin, A., Haeberli, W., 2020. Glacial lake depth and volume estimation based on a large bathymetric dataset from the Cordillera Blanca, Peru. In: Earth Surface Processes and Landforms. https://doi.org/10.1002/esp.4826.
Niggli, P., de Quervain, F.D., 1936. Geotechnische Karte der Schweiz. In: Schweizerische Geotechnische Kommission, Kummerly and Frey. Geotechnischer Verlag, Bern.
Patton, H., Swift, D.A., Clark, C.D., Livingstone, S.J., Cook, S.J., 2016. Distribution and characteristics of overdeepenings beneath the Greenland and Antarctic ice sheets: implications for overdeepening origin and evolution. Quat. Sci. Rev. 148, 128–145. https://doi.org/10.1016/j.quascirev.2016.07.012.
Patton, H., Swift, D.A., Clark, C.D., Livingstone, S.J., Cook, S.J., Hubbard, A., 2015. Automated mapping of glacial overdeepenings beneath contemporary ice sheets: approaches and potential applications. Geomorphology 232, 209–223. https://doi.org/10.1016/j.geomorph.2015.01.003.
Penck, A., 1905. Climatic features in the land surface. Am. J. Sci. 19 (110), 165–174.
Prasicek, G., Larsen, I.J., Montgomery, D.R., 2015. Tectonic control on the persistence of glacially sculpted topography. Nat. Commun. 6 https://doi.org/10.1038/ncomms9028.
Preusser, F., Reitner, J.M., Schlüchter, C., 2010. Distribution, geometry, age and origin of overdeepened valleys and basins in the Alps and their foreland. Swiss J. Geosci. 103, 407–426. https://doi.org/10.1007/s00015-010-0044-y.
Reber, R., Schlunegger, F., 2016. Unravelling the moisture sources of the Alpine glaciers using tunnel valleys as constraints. Terra. Nova 28, 202–211. https://doi.org/10.1111/ter.12211.
Röthlisberger, H., Iken, A., 1981. Plucking as an effect of water-pressure variations at the glacier bed. Ann. Glaciol. 2, 57–62. https://doi.org/10.3189/172756481794352144.
Seguinot, J., Ivy-Ochs, S., Jouvet, G., Huss, M., Funk, M., Preusser, F., 2018. Modelling last glacial cycle ice dynamics in the Alps. Cryosphere 12, 3265–3285. https://doi.org/10.5194/tc-12-3265-2018, 2018.
Shuster, D.L., Cuffey, K.M., Sanders, J.W., Balco, G., 2011. Thermochronometry reveals headward propagation of erosion in an alpine landscape. Science (80- 332, 84–88. https://doi.org/10.1126/science.1198401.
Sommaruga, A., Eichenberger, U., Marillier, F., 2012. Seismic atlas of the Swiss Molasse Basin. In: Edited by the Swiss Geophysical Commission. Matér. pour la Géol. la Suisse–Géophys, vol. 44, pp. 1–88.
Steinemann, O., Ivy-Ochs, S., Grazioli, S., Luetscher, M., Fischer, U.H., Vockenhuber, C., Synal, H.A., 2020. Quantifying glacial erosion on a limestone bed and the relevance for landscape development in the Alps. Earth Surf. Process. Landforms. https://doi.org/10.1002/esp.4812.
Sternai, P., Herman, F., Valla, P.G., Champagnac, J.D., 2013. Spatial and temporal variations of glacial erosion in the Rhone valley (Swiss Alps): insights from numerical modeling. Earth Planet Sci. Lett. 368, 119–131. https://doi.org/10.1016/j.epsl.2013.02.039.
Swift, D.A., Persano, C., Stuart, F.M., Gallagher, K., Whitham, A., 2008. A reassessment of the role of ice sheet glaciation in the long-term evolution of the East Greenland fjord region. Geomorphology 97, 109–125. https://doi.org/10.1016/j.geomorph.2007.02.048.
Ugelvig, S.V., Egholm, D.L., Anderson, R.S., Iverson, N.R., 2018. Glacial erosion driven by variations in meltwater drainage. J. Geophys. Res. Earth Surf. 123, 2863–2877. https://doi.org/10.1029/2018JF004680.
Ugelvig, S.V., Egholm, D.L., Iverson, N.R., 2016. Journal of Geophysical Research: Earth Surface Glacial Landscape Evolution by Subglacial Quarrying: A Multiscale Computational Approach, pp. 1–27. https://doi.org/10.1002/2016JF003960.Abstract.
Wang, J., Yao, P., Yu, B., Zou, L., Wang, F., Harbor, J.M., 2018. Controls on spatial variations of glacial erosion in the Qilian Shan, northeastern Tibetan Plateau. Geomorphology 318, 128–138. https://doi.org/10.1016/j.geomorph.2018.06.004.